

1 **Plastid phylogenomics reveals evolutionary relationships in the** 2 **mycoheterotrophic orchid genus *Dipodium* and provides** 3 **insights into plastid gene degeneration**

4
5 **Stephanie Goedderz^{1,2,*}, Mark A. Clements³, Stephen J. Bent⁴, James A. Nicholls⁵,**
6 **Vidushi S. Patel⁶, Darren M. Crayn¹, Philipp M. Schlüter², Katharina Nargar^{1,6,*}**
7

8 ¹ Australian Tropical Herbarium, James Cook University, PO Box 6811, Cairns, QLD 4870,
9 Australia.

10 ² Department of Plant Evolutionary Biology, Institute of Biology, University of Hohenheim,
11 Stuttgart, Germany.

12 ³ Centre for Australian National Biodiversity Research (joint venture between Parks Australia
13 and CSIRO), GPO Box 1700, Canberra, ACT 2601, Australia.

14 ⁴ Data61, Commonwealth Industrial and Scientific Research Organisation (CSIRO), GPO Box
15 2583, Brisbane, QLD 4001, Australia.

16 ⁵ Australian National Insect Collection, Commonwealth Industrial and Scientific Research
17 Organisation (CSIRO), GPO Box 1700, Canberra, ACT 2601, Australia.

18 ⁶ National Research Collections Australia, Commonwealth Industrial and Scientific Research
19 Organisation (CSIRO), GPO Box 1700, Canberra, ACT 2601, Australia.

20 21 *** Correspondence:**

22 Stephanie Goedderz
23 stephanie.goedderz@jcu.edu.au
24 Katharina Nargar
25 katharina.nargar@csiro.au

26 **Keywords:** *Dipodium*, divergence-time estimation, gene degradation, mycoheterotrophy,
27 phylogenetics, plastome

28 **Abstract**

29 The orchid genus *Dipodium* R.Br. (Epidendroideae) comprises leafy autotrophic and leafless
30 mycoheterotrophic species, the latter confined to sect. *Dipodium*. This study examined
31 plastome degeneration in *Dipodium* in a phylogenomic and temporal context. Whole plastomes
32 were reconstructed and annotated for 24 *Dipodium* samples representing 14 species and two
33 putatively new species, encompassing over 80% of species diversity in sect. *Dipodium*.
34 Phylogenomic analysis based on 68 plastid loci including a broad outgroup sampling across

35 Orchidaceae found sect. *Leopardanthus* as sister lineage to sect. *Dipodium*. *Dipodium*
36 *ensifolium*, the only leafy autotrophic species in sect. *Dipodium* was found sister to all leafless,
37 mycoheterotrophic species, supporting a single evolutionary origin of mycoheterotrophy in the
38 genus. Divergence time estimations found that *Dipodium* arose ca. 33.3 Ma near the lower
39 boundary of the Oligocene and crown diversification commenced in the late Miocene, ca. 11.3
40 Ma. Mycoheterotrophy in the genus was estimated to have evolved in the late Miocene, ca. 7.3
41 Ma, in sect. *Dipodium*. The comparative assessment of plastome structure and gene degradation
42 in *Dipodium* revealed that plastid *ndh* genes were pseudogenised or physically lost in all
43 *Dipodium* species, including in leafy autotrophic species of both *Dipodium* sections. Levels of
44 plastid *ndh* gene degradation were found to vary among species as well as within species,
45 providing evidence of relaxed selection for retention of the NADH dehydrogenase complex
46 within the genus. *Dipodium* exhibits an early stage of plastid genome degradation as all species
47 were found to have retained a full set of functional photosynthesis-related genes and
48 housekeeping genes. This study provides important insights into plastid genome degradation
49 along the transition from autotrophy to mycoheterotrophy in a phylogenomic and temporal
50 context.

51 **1 Introduction**

52 Heterotrophic plants - plants that rely on other organisms for energy and nutrients - are
53 remarkable survivors, exhibiting often curious morphological, physical, or genomic
54 modifications, reflecting evolutionary relaxed selective pressure on photosynthetic function
55 (Graham et al., 2017; Barrett et al., 2019). Advances in next generation sequencing and
56 bioinformatic pipelines have vastly accelerated the characterisation of plastid genomes
57 (plastomes), including of heterotrophic plants, providing new insights into plastome evolution.
58 Plastomes of heterotrophic plants often exhibit greatly altered structure and gene content due
59 to photosynthesis-related genes that are no longer required (Delannoy et al., 2011; Barrett et
60 al., 2014; Lam et al., 2015; Graham et al., 2017; Braukmann et al., 2017; Barrett et al., 2018;
61 Wicke and Neumann 2018; Qu et al., 2019; Barrett et al., 2019; Klimpert et al., 2022; Peng et
62 al., 2022; Wen et al., 2022). Hence, heterotrophic plants offer excellent opportunities to gain
63 insight into plastome evolution under relaxed selection.

64 Early non-phylogenomic studies on plastome evolution in heterotrophic plants allowed the
65 discovery of large-scale plastome evolutionary patterns and, moreover, stimulated research into
66 fine-scale, phylogenetic comparative approaches (e.g., Delannoy et al., 2011; Logacheva et al.,
67 2011; Roma et al., 2018). Thus far, most phylogenetic comparative studies included plastomes
68 of taxa scattered across families, tribes, or genera (e.g., Kim et al., 2015; Feng et al., 2016; Niu
69 et al., 2017; Lallemand et al., 2019; Li et al., 2020; Kim et al., 2020; Tu et al., 2021; Kim et
70 al., 2023). Yet, phylogenetic, comparative approaches at infrageneric level are still scarce (e.g.,
71 Barrett et al., 2018; Barrett et al., 2019).

72 Orchidaceae, one of the two largest flowering plant families, has undergone a greater number
73 of independent transitions from autotrophy to heterotrophy than any other land plant lineage
74 (Merckx 2013; Christenhusz and Byng 2016; Jacquemyn and Merckx 2019). The family
75 comprises several heterotrophic orchid lineages which rely to some extent on mycorrhizal fungi
76 for carbon and other nutrients i.e., initial, partial, or full mycoheterotrophy (Merckx 2013).

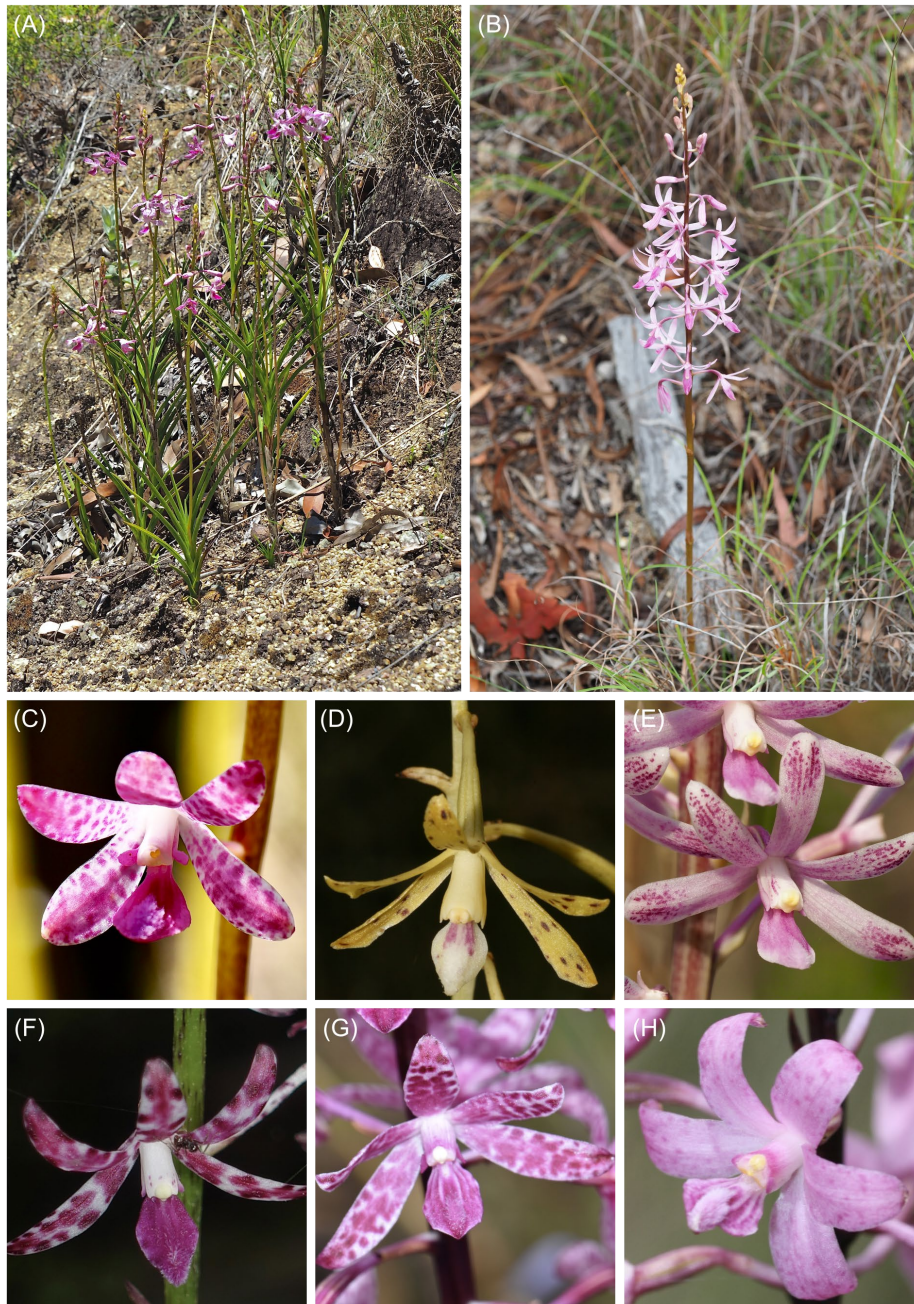
77 So far, most examined mycoheterotrophic orchid plastomes exhibited degradation patterns
78 similar to those found in heterotrophic plastomes of other plants. These include a reduction in
79 genome size, decrease in guanine-cytosine (GC) content, rearrangements, pseudogenisations
80 and gene losses (e.g., Delannoy et al., 2011; Barrett et al., 2018; Lallemand et al., 2019; Barrett
81 et al., 2019; Wen et al., 2022). Moreover, whole plastome sequencing has revealed patterns of
82 plastid gene degradation for various heterotrophic plastomes which led to the development of

83 conceptual models to predict the evolutionary transition from autotrophy to heterotrophy of the
84 plastid organelle (e.g., Graham et al., 2017; Barrett et al., 2019). Several studies in
85 mycoheterotrophic orchid lineages found support for these models which predict a progression
86 from losses of the chloroplast *ndh* genes to genes encoding complexes which are directly
87 involved in photosynthesis (e.g., *psa*, *psb*) to more general ‘housekeeping’ genes (e.g., *accD*,
88 *matK*) (Wicke and Naumann 2018; Barrett et al., 2018; Barrett et al., 2019; Kim et al., 2020;
89 Kim et al., 2023).

90 Interestingly, degraded *ndh* genes were also found in some autotrophic orchids (e.g., Kim et
91 al., 2015; Niu et al., 2017; Kim and Chase 2017; Lallemand et al., 2019; Kim et al., 2023). This
92 appears curious, as the *ndh* genes encode proteins of the NADH dehydrogenase complex (NDH
93 complex) which is assumed to play a role in cyclic electron flow and thus fine-tunes
94 photosynthesis (Yamori et al., 2015; Peltier et al., 2016). Degradation of *ndh* genes is
95 hypothesised to have led to additional structural changes of the plastome (Kim et al. 2015). In
96 particular, *ndhF* gene loss was correlated with shifts in the position of the junction of the
97 inverted repeat/small single copy (IR/SSC) region in Orchidaceae and other plants (Kim et al.,
98 2015; Niu et al., 2017; Dong et al., 2018; Roma et al., 2018; Thode and Lohmann 2019; Li et
99 al., 2021; Könyves et al., 2021). However, within Orchidaceae, degradation of *ndh* genes was
100 found to vary even among closely related species (e.g., Kim et al., 2015; Feng et al., 2016; Kim
101 and Chase, 2017; Barrett et al., 2018; Barrett et al., 2019) which suggests the genes for the
102 NDH complex may be under relaxed selective pressure in several orchid lineages (Kim and
103 Chase, 2017). Moreover, previous studies found that *ndh* degradation patterns vary
104 considerably and have been independently degraded among orchids (Kim et al., 2015; Niu et
105 al., 2017; Kim and Chase 2017; Lallemand et al., 2019).

106 The orchid genus *Dipodium* R.Br. (Cymbidieae) contains both autotrophic and
107 mycoheterotrophic species and thus represents a suitable model system in which to address
108 hypotheses of plastome evolution. The genus comprises 39 species and is divided into two
109 sections, *Dipodium* and *Leopardanthus* (Blume) O. Kuntze, based on morphological and
110 geographical evidence (O’Byrne, 2017; Jones, 2021). Sect. *Leopardanthus* (26 species) is
111 distributed in the floristic regions of Malesia and Australasia (O’Byrne, 2017). All species of
112 sect. *Leopardanthus* are green leafy plants and non-uniform in habit (O’Byrne, 2017). Section
113 *Dipodium* occurs predominantly in Australasia, with nearly all species being endemic in
114 Australia. One species occurs in New Guinea (*D. elatum* J.J.Sm.), one species extends into the
115 Pacific region (*D. squamatum* (G.Forst.) Sm. (New Caledonia and Vanuatu), and one occurs
116 in Malesia (*D. gracile* Schltr. (Sulawesi) (Schlechter, 1911; O’Byrne, 2017; POWO, 2023;

117 WFO, 2023). In contrast to sect. *Leopardanthus*, most species of sect. *Dipodium* are non-
118 climbing terrestrials, forming subterranean rhizomes and erect flowering stems with highly
119 reduced, non-photosynthetic leaves (i.e., scales) (**Figure 1, B**). Hence, species within sect.
120 *Dipodium* are generally assumed to be fully mycoheterotrophic (O'Byrne, 2014). However,
121 one Australian species of sect. *Dipodium*, *D. ensifolium* F.Muell., stands out as a leafy
122 terrestrial (**Figure 1, A**).
123



124 **Figure 1:** Habit and flowers of *Dipodium* sect. *Dipodium*. A. *D. ensifolium*; B. *D. elegantulum* (note
125 the green to purplish inflorescence stem); C. *D. ensifolium*; D. *D. interaneum*; E. *D. elegantulum*; F. *D.*
126 *variegatum*; G. *D. punctatum*; H. *D. roseum*. (Photos: A-C, E: S. Goedderz; D, F -H: M.A. Clements.)
127
128

129 The aims of this study were to:

- 130 1. sequence and assemble plastid genomes for species of *Dipodium* to elucidate patterns of
131 plastid genome modification (e.g., rearrangement, structural variation, pseudogenisation,
132 gene loss) across autotrophs and mycoheterotrophs within the genus and examine gene
133 degradation in context of current models of plastome degradation in heterotrophic plants.
- 134 2. infer phylogenomic relationships within section *Dipodium* and among closely related
135 autotrophic relatives (i.e., *Dipodium* section *Leopardanthus*).
- 136 3. estimate divergence times of *Dipodium* to assess the origin of mycoheterotrophy within the
137 genus and elucidate over which evolutionary timeframes plastid gene degradation and
138 losses has taken place within *Dipodium*.

139 **2 Material and methods**

140 **2.1 Plant material**

141 For this study, we sampled all known Australian species of section *Dipodium* and one
142 representative of section *Leopardanthus* (**Table 1**). Based on previous molecular systematic
143 studies (Serna-Sánchez et al., 2021; Pérez-Escobar et al. 2023; Zhang et al. 2023), an extended
144 outgroup from closely related orchid genera within subtribe Eulophiinae (*Eulophia* R.Br.,
145 *Geodorum* Andrews) and subtribe Cymbidiinae (*Cymbidium* Sw., *Acriopsis* Reinw. ex. Blume)
146 was sampled (**Table 1**). Specimens studied were from different regions within Australia, with
147 the exception of one specimen from Papua New Guinea (*D. pandanum* 2) (**Table 1**).

148 **2.2 DNA extraction, library preparation, and sequencing**

149 Standard plant DNA extractions were carried out from 5-20 mg of silica dried plant tissue from
150 field collections or herbarium material (**Table 1**) at the National Research Collections Australia
151 (NRCA, CSIRO) in Canberra. The Invisorb DNA Plant HTS96 kit (Stratec, Birkenfeld,
152 Germany) was used following the manufacturer's protocol, with a final elution of 60 ml.

153 DNA of *Dipodium* samples (**Table 1**) was sonicated to an average target length of ca. 200 bp
154 using a LE220 sonicator (Covaris, Bankstown, Australia). After sonication, DNA length and
155 concentration were quantified on Fragment Analyzer (Agilent Technologies, California, USA)
156 using the Agilent high-sensitivity genomic DNA kit.

157 DNA libraries were prepared using the QiaSeq UltraLow Input library kit (Qiagen,
158 Germantown, Australia) using custom dual-indexed adapters. Final libraries were size-selected
159 on Fragment Analyzer using the high-sensitivity Genomic Fragment Analyzer Kit (Agilent,
160 Santa Clara, USA), quantified using the Fluoroskan plate fluorometer (Thermo Fisher

161 Massachusetts, USA) and the Quant-iT HS dsDNA kit (Invitrogen, California, USA) following
162 the manufacturer's instructions. Samples were pooled equimolarly and sequenced using 150
163 bp paired end reads on a NovaSeq S1 flowcell (Illumina, California, USA) at the Biomolecular
164 Resource Facility within the John Curtin School of Medical Research, Australian National
165 University (Canberra, Australia).

166 **2.3 Data processing and whole plastid genome assembly**

167 We carried out both *de novo* and reference-guided assemblies for the *Dipodium* data set.
168 Trimming and assembly of *de novo* contigs were carried out as described in Nargar et al.
169 (2022). Briefly, raw sequences were trimmed applying a Phred score > 20 using Trimmomatic
170 0.39 (Bolger et al., 2014), and deduplicated using 'clumpify' from BBtools 38.9 (Bushnell,
171 2014). Read pairs were then assembled using SPAdes 3.15 (Bankevich et al., 2012). Plastid
172 databases were extracted from NCBI's Nucleotide Entrez database using Entrez Programming
173 Utilities (2008) using taxonomic, keyword, and sequence length constraints. Contigs were
174 identified as derived from plastid source using blastn against these databases. Genes within
175 plastid contigs were identified by homology using BLAST (Altschul et al., 1990) and BLASTx
176 (RRID:SCR_001653) against genes extracted from annotations of the reference sequence sets
177 extracted from nuccore.

178 Reference-guided assemblies were performed with paired, merged reads and the recently
179 published and closely related plastome of *Dipodium roseum* D.L.Jones and M.A.Clem.
180 (MN200386, Kim et al., 2020). The related orchid *Masdevallia coccinea* Linden ex Lindl.
181 (KP205432, Kim et al., 2015) was included as an additional reference sequence to ensure that
182 regions which already showed degradation in some plastid genes in the plastome of *D. roseum*
183 (e.g., all *ndh* genes) (MN200386, Kim et al., 2020) and which may still be present in other
184 *Dipodium* species could be assembled as the plastome of *M. coccinea* has a full set of functional
185 plastid genes (Kim et al., 2015).

186 Reference-guided assemblies were carried out using the plugin 'map to reference' in Geneious
187 Prime (Version 2022.0.2, Biomatters Ltd, www.geneious.com) with default settings. To obtain
188 complete plastome assemblies, consensus sequences for each sample were extracted (threshold
189 60%, reading depth > 10), aligned using MAFFT v7.388 (Katoh and Standley 2013) in
190 Geneious, manually checked and compared. Reference-guided assemblies were visually
191 inspected and in cases of misassembled regions due to potential mismatches between the
192 sample and the reference *de novo* assemblies were consulted, and were quality allowed the
193 region extracted from the *de novo* assembly. The prediction and finding of gene annotations

194 for complete plastome assemblies were performed with the Geneious plugin ‘predict
195 annotation’ (similarity: 90% and best match with *D. roseum* (MN200386)). Open reading
196 frames (ORFs) were manually checked and verified by identifying the start and stop codons.
197 In cases of remaining ambiguities, BLAST searches were conducted for reading-frame
198 verification (Altschul et al. 1990; National Center for Biotechnology Information; Available
199 from: <https://blast.ncbi.nlm.nih.gov/Blast.cgi> [cited: 08 Sept 2023]). The inverted repeat (IR)
200 boundaries were identified using the ‘repeat finder’ plugin in Geneious with default settings.
201 In total, 24 complete *Dipodium* plastomes were assembled in this study. The graphical
202 representation of each plastome and divergent regions with annotations were created in
203 OrganellarGenomeDRAW (OGDRAW, version 1.3.1, Greiner et al., 2019).

204 **2.4 Phylogenetic analyses**

205 To elucidate phylogenetic relationships within *Dipodium* and to assess the phylogenetic
206 position of *Dipodium* within Cymbidieae we performed a phylogenetic analysis with DNA
207 sequences of 33 newly sequenced plastomes from this study (**Table 1**) and an extended
208 outgroup sampling for 115 samples from published plastid data (Supplementary Material 1).

209 Coding regions of respective genes of 33 samples were extracted with the ‘extract’ function in
210 Geneious Prime. Where mutations had led to frame shifts with internal stop codons, the
211 affected sequences were excluded from phylogenetic analyses.

212 Each extracted coding region of in total 68 plastid loci from 33 samples (including the intron
213 regions) and from 115 published plastomes (excluding intron regions) were aligned using
214 MAFFT (v7.388; Katoh et al., 2002; Katoh and Standley 2013) Geneious prime plugin with
215 default settings, checked manually and subsequently concatenated to an alignment of 69,335
216 bp (Supplementary Material 2).

217 Maximum likelihood analysis of the plastid dataset (148 samples) with best-fit models
218 GTR+I+I+F+R4 was performed using IQ-TREE ver. 2.2.0 (Nguyen et al., 2015;
219 Kalyaanamoorthy et al., 2017; Minh et al., 2020). Branch support was obtained with
220 Shimodaira-Hasegawa-like approximate Likelihood Ratio Test (SH-aLRT; Guindon et al.,
221 2010) and the ultrafast bootstrap (ufboot2; Hoang et al., 2018) as implemented in the IQ-TREE
222 software. The tree topology was visualised using the software Figtree (ver. 1.4.4.;;
223 <http://tree.bio.ed.ac.uk/software/figtree/>).

224

225

226 2.5 Divergence-time analysis

227 For divergence-time estimations of *Dipodium*, the alignments were reduced to the 30 most
228 parsimony informative loci due to computational limitations. The 30 plastid loci were selected
229 based on their most parsimony informative (Pi) sites estimated with MEGA (Molecular
230 Evolutionary genetics Analysis; ver. 11.0.11, Tamura et al., 2021) and presence of loci across
231 the dataset (Supplementary Material 2). For taxa represented by more than one sample,
232 duplicates were removed from alignments as recommended for divergence time estimation.
233 Alignments of 30 plastid loci from 134 taxa were concatenated yielding a total alignment length
234 of 27,934 bp using MAFFT (v7.388; Katoh et al., 2002; Katoh and Standley 2013)
235 implemented in Geneious Prime (Supplementary Material 2). Absolute node ages and
236 phylogenetic relationships were jointly estimated in BEAST (ver. 2.7.4; Bouckaert et al., 2019,
237 Bouckaert et al. 2014) applying the best fit partition scheme and substitution model as
238 determined by IQ-TREE's ModelFinder (GTR+F+I+R4). Four different models were tested:
239 a Bayesian optimised relaxed and a strict molecular clock with uncorrelated lognormal rates
240 with each a Yule and a Birth-death tree prior on the speciation process (Douglas et al., 2021;
241 Gernhard et al., 2008; Zuckerkandl and Pauling, 1965; Yule, 1925). Trees were calibrated with
242 four secondary calibration points based on Zhang et al. (2023). A normal distribution with an
243 offset value of 101.52 Ma and a standard deviation (SD) of 2.2 was assigned as crown age of
244 Orchidaceae. The priors for the three other calibration points were set with a normal
245 distribution and the means of stem ages for Vanilloideae (offset value = 93.48 Ma, SD = 2.7),
246 Cyripedioideae (offset value = 89.14 Ma, SD = 2.71) and Orchidoideae (offset value = 77.74
247 Ma, SD = 2.0). For each clock model, 10 parallel BEAST analyses with each 30 million
248 generations and a sampling frequency of every 10,000 generations were carried out. The run
249 parameters were examined in TRACER (ver. 1.7.2; Rambaut et al., 2018) and the effective
250 sample sizes (ESSs) of > 200 for all parameters and the burn-in were assessed. The runs were
251 combined in LogCombiner (Drummond and Rambaut 2007) with a burn-in of 10% and
252 subsequently used to generate a maximum-clade-credibility chronogram with mean node
253 heights in TreeAnnotator (Drummond and Rambaut 2007). To determine the best fitting clock
254 model and speciation models for the data set, a model comparison using the AICM (Akaike
255 Information Criterion by MCMC) was performed with BEAST v.2.6.2 and evaluated with the
256 AIC model selection criterion of Fabozzi et al. (2014).

257

258

259 2.6 Plastid genome evolution

260 2.6.1 Structural variation in *Dipodium* plastomes

261 To examine structural variation among the plastomes of *Dipodium*, whole plastome alignments
262 were generated using MAFFT (v7.388; Katoh et al., 2002; Katoh and Standley 2013)
263 implemented in Geneious Prime with full annotations. Alignments were manually checked, in
264 cases of divergent regions e.g., the operon region of *ndhC*, *ndhK*, and *ndhJ* genes or junctions
265 between the large single copy (LSC)/ inverted repeat B (IRB)/ small single copy (SSC)/
266 inverted repeat A (IRA) regions, and respective regions (including annotations) were extracted
267 in Geneious Prime, separately aligned, proofread, and subsequently visualised using
268 OGDRAW (ver. 1.3.1, Greiner et al., 2019).

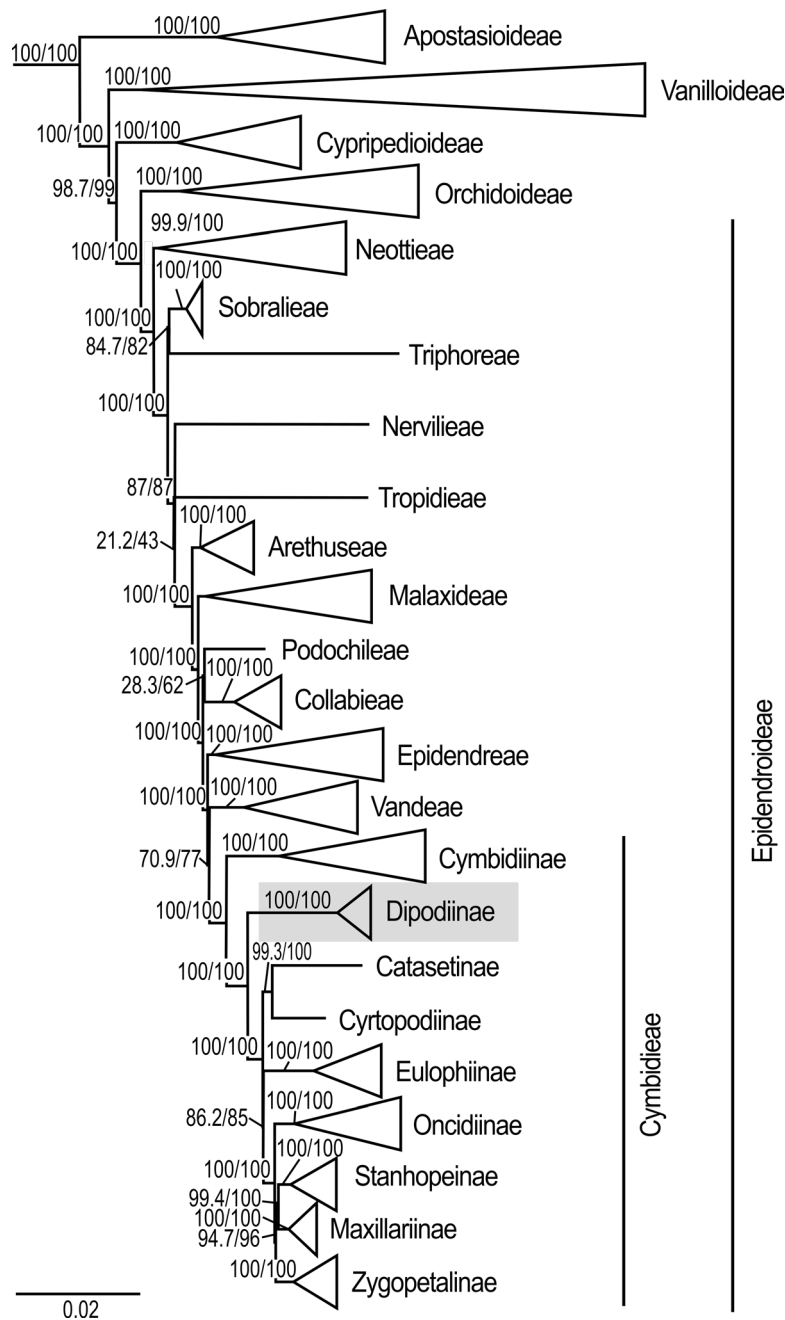
269 2.6.2 Functional genes, pseudogenes, and physical gene loss

270 To classify the level of degradation of plastid genes in *Dipodium*, we used the following
271 categories: (1) **functional** - the reading frame was intact and less than 10% of the open reading
272 frame was disrupted by small indels; (2) **moderately pseudogenised** - less than 10% of the open
273 reading frame was disrupted by internal stop codons or indels causing non-triplet frame shifts;
274 (3) **severely pseudogenised** - more than 10% of the open reading frame was disrupted by either
275 internal stop codons, large deletions (> 10%), and non-triplet frame shifts (based on Barrett et
276 al., 2019), or (4) **lost** - the gene was not identified in the annotation process of the *de-novo*
277 assembly (e.g., Joyce et al., 2018) and/or was not detectable within the reference-guided
278 assembly. A gene was considered as not detectable within the reference-guided mapping
279 process if at least 70% of the gene sequence could not be identified for calculation of the
280 consensus sequence within the Geneious mapping process. The coded matrix of gene
281 degradation was plotted against the maximum likelihood phylogenetic tree of *Dipodium*.

282 3 Results

283 3.1 Phylogenetic placement of *Dipodium* in tribe Cymbidieae and infrageneric 284 relationships within the genus

285 The maximum likelihood analysis based on 68 plastid loci and 148 samples yielded highly
286 resolved and well-supported tree topologies for the phylogenomic relationships within
287 Orchidaceae (Supplementary Material 3). Within Epidendroideae, Cymbidiinae was
288 monophyletic and sister to all other Cymbidieae including Dipodiinae (SH-aLRT/UFboot
289 100/100; **Figure 2**). *Dipodium* was retrieved as next diverging lineage within Cymbidieae and
290 monophyletic with maximum support values (SH-aLRT/UFboot 100/100; **Figure 2**).



291

292 **Figure 2:** Phylogenetic relationships among major orchid lineages and placement of subtribe
 293 *Dipodiinae* in Cymbidieae. Maximum likelihood tree of 148 taxa based on 68 plastid loci. Support
 294 values are shown above each branch, SHaLRT followed by UFboot values. Scale bar represents branch
 295 length, along which 0.02 per-site substitutions are expected. Detailed phylogeny provided in
 296 Supplementary Material 3.

297

298 Within *Dipodium*, section *Leopardanthus* was placed as sister group to section *Dipodium* with
 299 maximum support values (SH-aLRT/UFboot 100/100; **Figure 3**).

300 Section *Dipodium* was resolved as monophyletic and divided into six highly supported
 301 lineages. The leafy species *D. ensifolium* was placed as sister to all leafless species of the
 302 section (SH-aLRT/UFboot 100/100; **Figure 3**). Next, sect. *Dipodium* split into two main

303 clades, A and B (SH-aLRT/UFboot 99/100; **Figure 3**). Clade A split into two lineages, the
 304 *Dipodium hamiltonianum* complex and the *Dipodium stenocheilum* complex, receiving
 305 maximum nodal support (SH-aLRT/UFboot 100/100; **Figure 3**). The *D. hamiltonianum*
 306 complex comprised the two species *D. hamiltonianum* and *D. interaneum*. The *D. stenocheilum*
 307 complex included *D. ammolithum*, *D. basalticum*, *D. elegantulum*, *D. stenocheilum*, and *D. aff.*
 308 *stenocheilum*. *Dipodium stenocheilum* was retrieved as non-monophyletic. (**Figure 3**).

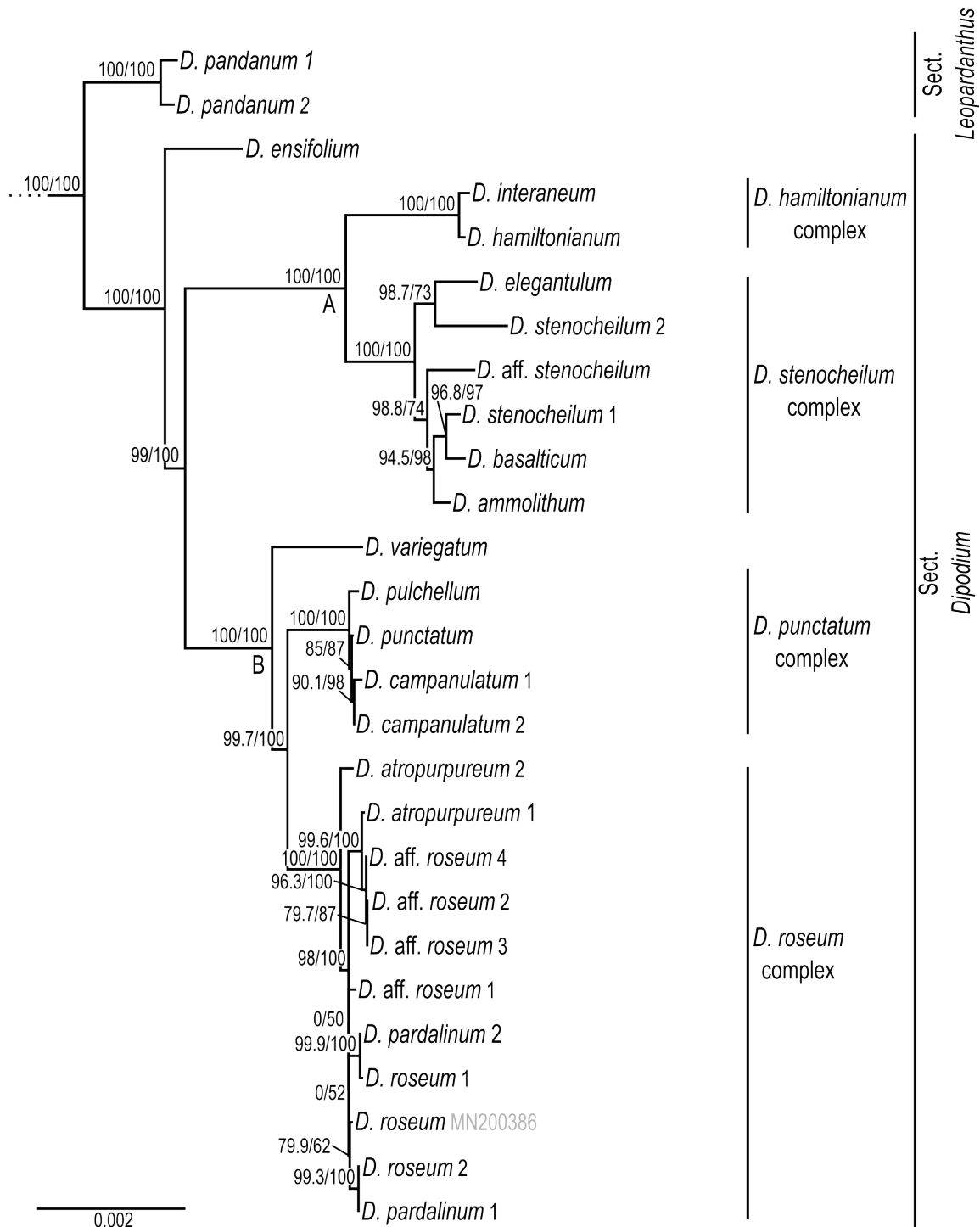


Figure 3: Phylogenetic relationships in *Dipodium*. Maximum likelihood tree based on 68 plastid loci and 148 taxa (outgroups not shown). Support values are given above each branch, SHaLRT is followed

312 by UFBoot values. Scale bar represents branch length, along which 0.002 per-site substitutions are
313 expected.

314

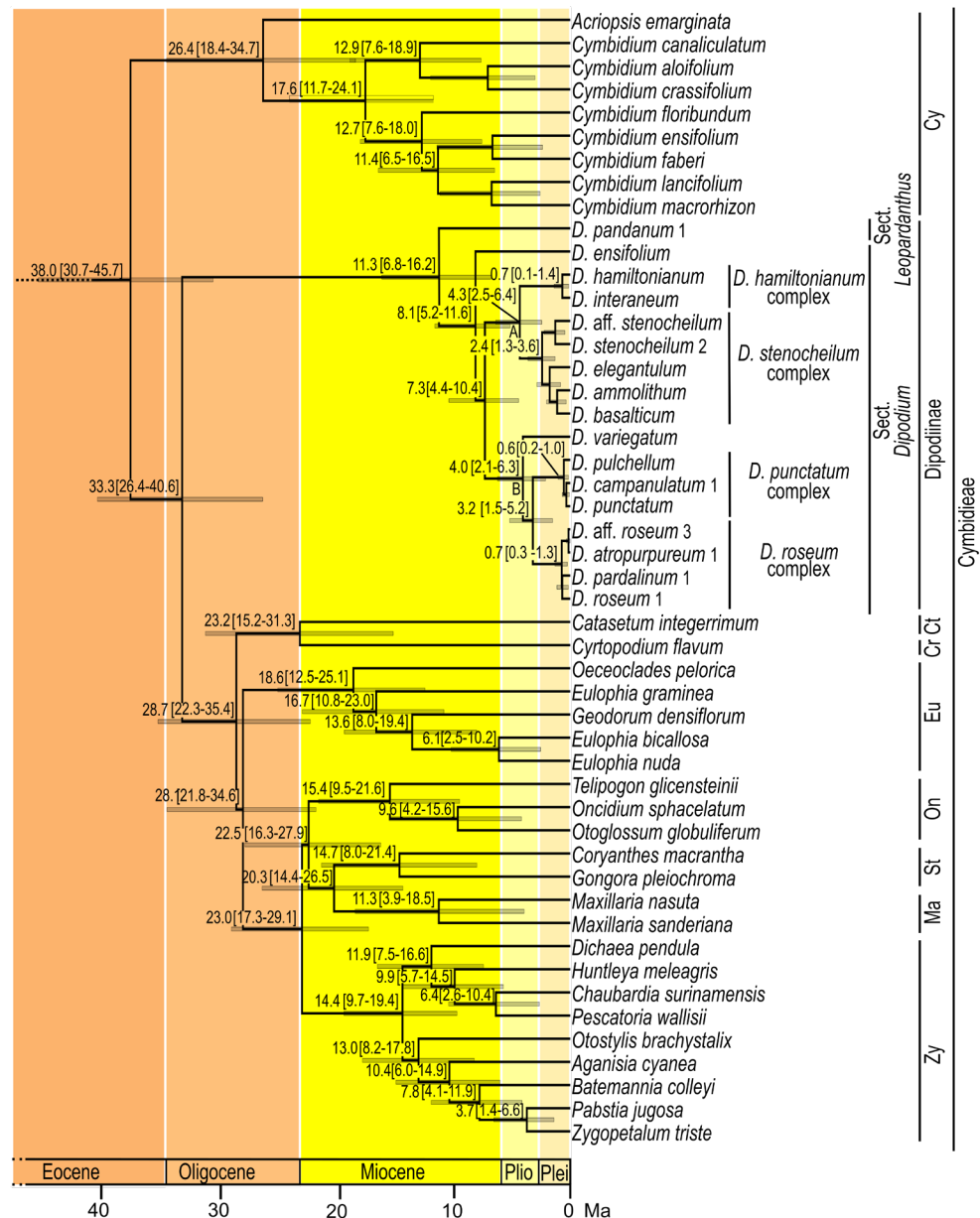
315 Clade B resolved *D. variegatum* as sister to the remaining species of the clade (SH-
316 aLRT/UFboot 100/100). The remainder split into the *D. punctatum* complex and the *D. roseum*
317 complex (SH-aLRT/UFboot 99.7/100; **Figure 3**). The *D. punctatum* complex comprised three
318 species, *D. campanulatum*, *D. pulchellum*, and *D. punctatum*. Phylogenetic divergence
319 between these three species was shallow and support for interspecific relationships within the
320 complex low. The *D. roseum* complex comprised four taxa, namely *D. atropurpureum*, *D.*
321 *pardalinum*, *D. roseum*, and *D. aff. roseum*. Resolution and support for interspecific
322 relationships within the *D. roseum* complex was low overall.

323 **3.2 Divergence-time estimations**

324 Absolute times of divergence under strict and optimised relaxed clocks for Orchidaceae based
325 on 30 plastid loci and 134 taxa showed similar results. Strict clock models consistently yielded
326 slightly older age estimates than the analyses based on the relaxed clock models
327 (Supplementary Material 4). Model comparison using AICM (Fabozzi et al., 2014) identified
328 the relaxed clock model under the birth-death speciation model as the best fit models for the
329 dataset (Supplementary Material 4).

330 The Bayesian relaxed clock tree topology and the maximum likelihood phylogeny agreed
331 overall in major relationships within Orchidaceae and the placement of species within
332 *Dipodium*. Epidendroideae were estimated to have emerged ca. 77.7 Ma (HDP: 74.2–81.5)
333 with the stem age of subtribe Cymbidieae placed in the Eocene, ca. 42.2 Ma (HDP: 34.3–50.1)
334 (Supplementary Material 4 and 5). The stem age of subtribe Cymbidiinae, the first diverging
335 lineage in Cymbidieae, was placed in the late Eocene, ca. 38.0 Ma (HDP: 30.7–45.7) (**Figure**
336 **4**). Stem diversification of Dipodiinae was estimated to have commenced ca. 33.3 Ma (HDP:
337 26.4–40.6) in the early Oligocene (**Figure 4**). Crown diversification of Dipodiinae was
338 estimated to have commenced much later, in the late Miocene with sections *Dipodium* and
339 *Leopardanthus* diverging ca. 11.3 Ma (HDP: 6.8–16.2) (**Figure 4**). The crown age of section
340 *Dipodium* was estimated to be ca. 8.1 Ma (HDP: 5.2–11.6) in the late Miocene with the
341 divergence of the leafy species, *D. ensifolium*, from the remainder of section *Dipodium* (**Figure**
342 **4**). The crown age of the remainder of the section, i.e., all leafless species, was estimated to ca.
343 7.3 Ma (HDP: 4.4–10.4) (**Figure 4**). Within this leafless clade, two subclades each containing
344 two species complexes were resolved. The crown age of the clade comprising the *D.*
345 *hamiltonianum* complex and the *D. stenocheilum* complex was estimated to ca. 4.3 Ma

346 (HDP:2.5–6.4) in the early Pliocene (**Figure 4**) which is congruent with estimations of the
 347 crown age of clade B (comprising *D. variegatum* and the two complexes *D. punctatum* and *D.*
 348 *roseum*) (**Figure 4**). The *D. stenocheilum* complex had a crown age of ca. 2.4 Ma (HDP: 1.3–
 349 3.6) in the early Pleistocene. The three remaining complexes had crown ages estimated to the
 350 mid Pleistocene (*D. hamiltonianum* complex: ca. 0.7 Ma, HDP: 0.1–1.4; *D. punctatum*
 351 *complex*: ca. 0.6 Ma, HDP: 0.2–1.0, and *D. roseum* complex: ca. 0.7 Ma, HDP: 0.3–1.3)
 352 (**Figure 4**).



353
 354 **Figure 4:** Chronogram of Cymbidiaceae. Maximum-clade-credibility tree from Bayesian divergence-time
 355 estimation in BEAST2 based on 30 plastid loci and an optimised lognormal molecular clock model
 356 under the birth-death prior (outgroups not shown). Divergence times (million years ago) are shown at
 357 each node, together with 95% highest posterior density (HDP) values indicated by grey bars and values
 358 in parentheses. A and B refers to the two main lineages within sect. *Dipodium*. Cy: Cymbidiinae, Ct:
 359 Catasetinae, Cr: Cyrtopodiinae, Eu: Eulophiinae, On: Oncidiinae, St: Stanhopeinae, Ma: Maxillariinae,

360 Zy: Zygotetaliae, Plio: Pliocene, Plei: Pleistocene. Outgroups to Cymbidieae not shown. Detailed
361 chronogram provided in Supplementary Material 5.

362 **3.3 Characterisation of *Dipodium* plastomes**

363 Complete plastome assemblies and annotations were successfully carried out for 24 *Dipodium*
364 samples, representing all Australian species of section *Dipodium* including two recently
365 discovered species of section *Dipodium* (*D. ammolithum* and *D. basalticum*), two putatively
366 new species of section *Dipodium* (*D. aff. roseum*, *D. aff. stenocheilum*) and one species of
367 section *Leopardanthus* (*D. pandanum*) (**Table 2**). Plastome assemblies for *D. pandanum* 2 and
368 *D. aff. stenocheilum* showed an insufficient mean coverage (<30) for non-coding regions which
369 caused unsolved gaps and ambiguous bases which could not be reliably resolved. The number
370 of paired-end, trimmed reads for the successfully assembled complete plastomes ranged from
371 332,604 (*D. pandanum* 1) to 27,999,734 (*D. pardalinum* 2) and the mean coverage ranged from
372 31x to 627x (Supplementary Material 6).

373 **3.3.1 Plastome features and structural variations within *Dipodium* plastomes**

374 Plastome sizes of *Dipodium* ranged from 142,949 bp (*D. variegatum*) to 152,956 bp (*D. aff.*
375 *roseum* 3) (**Table 2, Figure 5**, Supplementary Material 7). The largest average plastome size
376 (150,578 bp) was found in the *D. roseum* complex, closely followed by the leafy *D. ensifolium*
377 (150,084 bp), and the *D. punctatum* complex (149,512 bp). Plastome sizes within the *D.*
378 *stenocheilum* complex were markedly lower with an average size of 146,305 bp. Similarly
379 small plastomes were also found in *D. hamiltonianum* (145,902 bp), *D. interaneum* (146,497
380 bp) and the leafy climber *D. pandanum* 1 (sect. *Leopardanthus*) (146,204 bp) (**Table 2**).
381 *Dipodium* plastomes possess the typical quadripartite structure of angiosperms, with the SSC
382 region ranging from 12,039 bp (*D. variegatum*) to 16,756 bp (*D. ensifolium*), the LSC region
383 ranging from 81,514 bp (*D. stenocheilum* 2) to 83,172 bp (*D. punctatum*), and the pair of IRs
384 ranging from 24,436 bp (*D. variegatum*) to 26,817 bp (*D. aff. roseum* 3) (**Table 2**).

385 Total mean GC content of *Dipodium* plastomes was 36.9%, ranging between 36.8% (*D. roseum*
386 2 and *D. pardalinum* 1) and 37.1% (*D. hamiltonianum*) (**Table 2**). Within the *D. roseum*
387 complex the GC content was 36.8% – 36.9%, followed by the *D. punctatum* complex (36.9%),
388 *D. stenocheilum* complex (37.0%) and the highest GC content was 37.1% and 37.0% (*D.*
389 *hamiltonianum* and *D. interaneum*) (**Table 2**).

390 The plastid genes of each plastome were rated as functional; moderately to severely
391 pseudogenised; or physically lost. The total number of functional genes in *Dipodium* plastomes
392 ranged slightly from 119 to 121 including a total of 73 or 74 functional protein-coding sequence

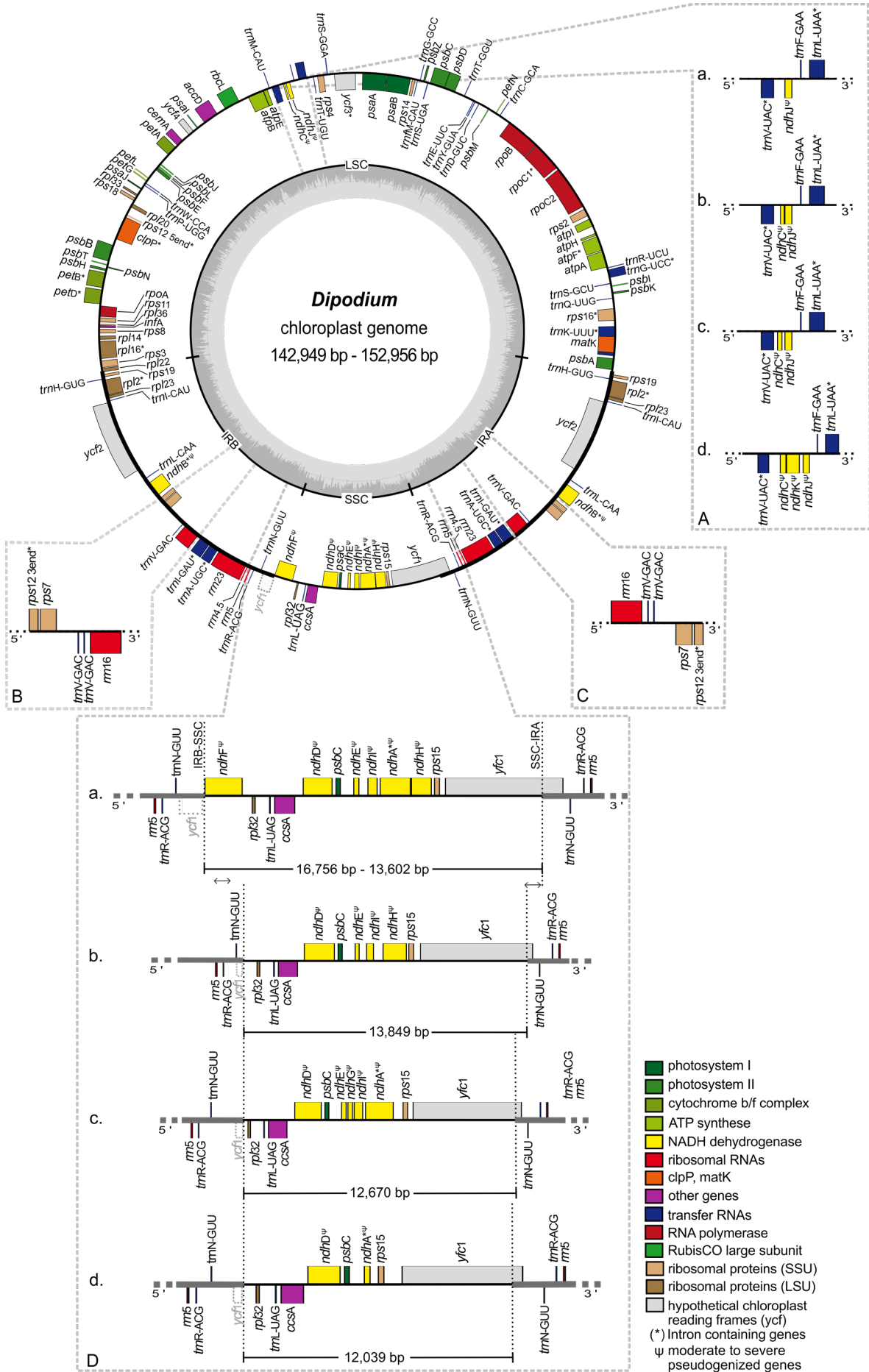
393 regions (CDS) (68 or 69 unique CDS), 37 to 39 functional tRNA genes (30 or 31 unique tRNA
394 genes) and 8 rRNA genes (4 unique rRNA genes) (**Table 2**).

395 The IR region was largely conserved among all examined *Dipodium* plastomes. All species
396 showed six duplicated coding regions in the IRs (i.e., *rpl2*, *rpl23*, *rps7*, *rps12*, *rps19*, *ycf2*) and
397 all four rRNA genes (**Table 3**). Most plastomes showed eight duplicated tRNA genes in the IR
398 regions with exception of the plastomes of *D. interaneum* and *D. elegantulum* which comprised
399 a duplicated *trnV*-GAC within the IRB and the plastomes of *D. ammolithum*, *D.*
400 *hamiltonianum*, and *D. stenocheilum* 2 which contained a duplicated *trnV*-GAC within the IRA
401 (**Table 3, Figure 5, B & C**). All plastomes contained 16 functional intron-genes (i.e., *atpF*,
402 *clpP*, *petB*, *petD*, *rpl2*, *rpl16*, *rpoC1*, *rps12*, *rps16*, *trnA*-UGC, *trnG*-UCC, *trnI*-GAU, *trnK*-
403 UUU, *trnL*-UAA, *trnV*-UAC, *ycf3*), except for *D. pandanum* 1 which possessed two
404 pseudogenes with introns (i.e., *ndhA*, *ndhB*) (**Table 3, Figure 5**). The *rps12* gene was trans-
405 spliced with the 5' end located in the LSC region and 3' end was duplicated in the IRs in all
406 studied plastomes (**Figure 5, Supplementary Material 7**).

407 The SSC region was found to vary the most among the examined samples. All plastomes
408 showed a contraction of the SSC with a reduction of 20-40% compared to the average size of
409 the angiosperm SSC regions (ca. 20 kb) (Ruhlman and Jansen 2014).

410 Three plastomes (*D. pandanum* 1, *D. stenocheilum* 1, *D. variegatum*) lost the *ndhF* gene. This
411 complete loss of the *ndhF* gene resulted in the *ycf1* fragment being located in the vicinity of
412 the *rpl32* (**Figure 5, D, b-d**) and caused a boundary shift of the IRB/SSC region located at the
413 3' end of the *ycf1* fragment and spacer region of *rpl32* (**Figure 5**). While all other plastomes
414 exhibited a severely truncated *ndhF* gene but did not exhibit an IRB/ SSC boundary shift
415 (**Figure 5, Supplementary Material 7**). The IRA/SSC junction in all examined plastomes was
416 located within the 5' portion of the functional *ycf1* gene, ranging from 97 bp (*D. pandanum* 1)
417 to 1,072 bp (*D. aff. roseum* 3) (**Figure 5**).

418 In contrast to the instability of the IR/SSC boundaries, IR/LSC boundaries were found to be
419 relatively stable. For all studied plastomes, the LSC/IRA boundaries were located near the 3'
420 end of *psbA* (**Figure 5**). Variations within the LSC regions were limited to the operon which
421 contained *ndhC*, J, K (**Figure 5, A**) and the independent pseudogenisation of *cemA* in the
422 plastome of *D. aff. roseum* 4 and *trnD*-GUC in the plastome of *D. campanulatum* (**Table 3,**
423 **Supplementary Material 7**).



425 **Figure 5:** Plastome map and boundary shifts in *Dipodium*. The plastome of *D. atropurpureum* 2 is
426 illustrated as representative and shown as a circular gene map with the smallest and the largest
427 *Dipodium* plastome of this study. Genes outside the circle are transcribed in a clockwise direction, those
428 inside the circle are transcribed in a counterclockwise direction. The dark grey inner circle corresponds
429 to the G/C content, and the lighter grey to the A/C content. The major distinct regions of complete
430 *Dipodium* plastomes are compared in each detailed enlarged box (A-D). (A) Note that each
431 representative block (a-d) has pseudogenised or lost either *ndhJ*, *ndhK* or *ndhC* genes. (B, C).
432 Duplication of *trnV*-GAC in the Inverted Repeat regions of *D. interaneum* (IRB), *D. hamiltonianum*
433 (IRA), *D. elegantulum* (IRB), *D. stenocheilum* 2 (IRA), *D. ammolithum* (IRA). (D) Each block (a. as
434 representative *D. roseum* 2; b. *D. pandanum* 1; c. *D. stenocheilum* 1; d. *D. variegatum*) shows
435 differences in the length (bp) of the SSC region caused through loss or pseudogenization of either *ndhF*,
436 *ndhD*, *ndhE*, *ndhG*, *ndhI*, *ndhA* or *ndhH*, note the boundary shift of the IRs/SSC region caused through
437 the loss/ pseudogenisation of *ndhF* and the inclusion of the functional *ycf1* and the *ycf1*-fragment (grey,
438 dashed line) into the IRs. SSC: Small Single Copy; LSC: Large Single Copy; IRA/B: Inverted Repeat
439 A/B.
440

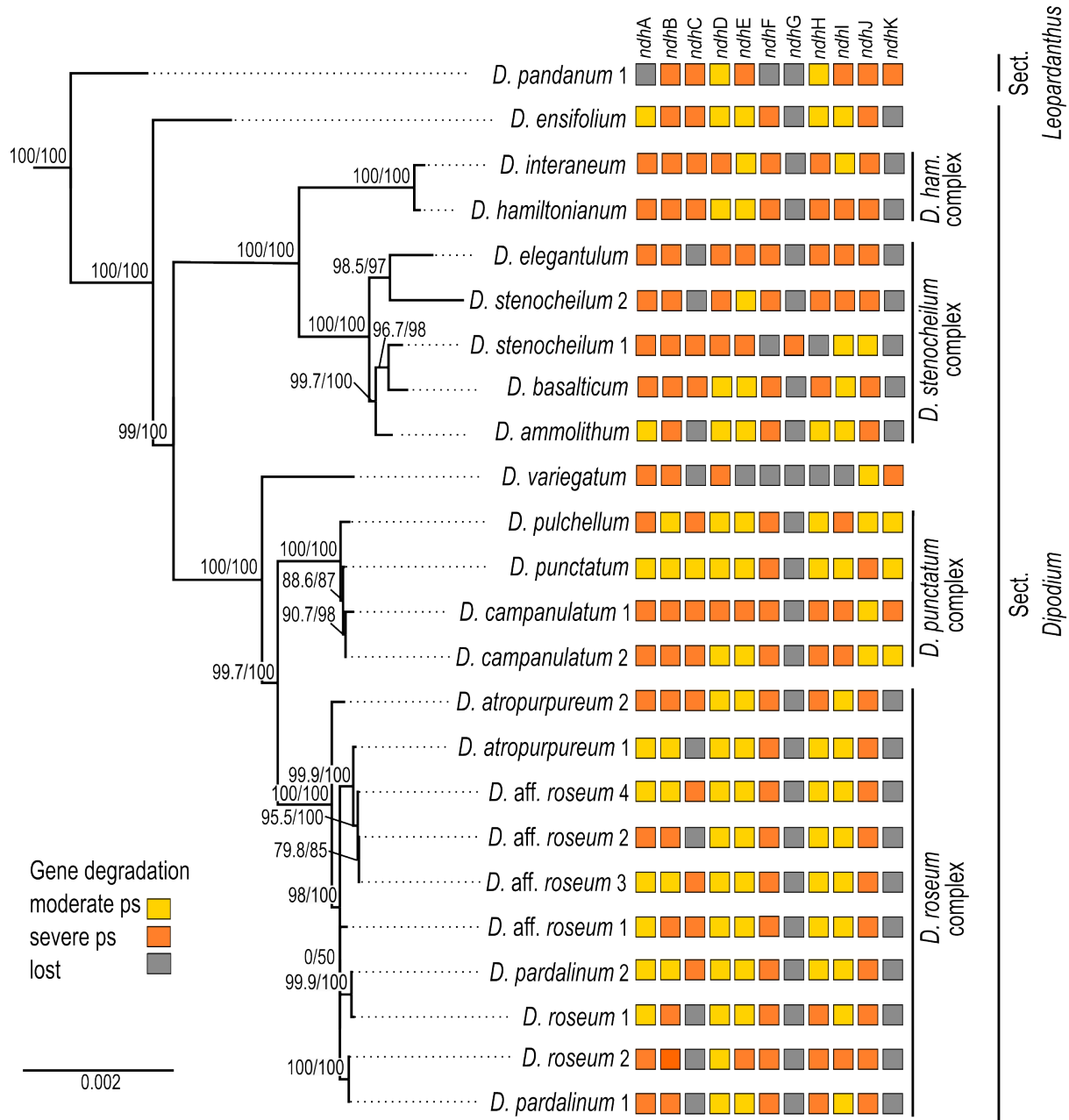
441 **3.3.2 *ndh* gene degradation and loss in *Dipodium***

442 All *ndh* genes exhibited varying degrees of putative loss or pseudogenisation; not a single *ndh*
443 gene remained functional in the examined *Dipodium* plastomes (**Table 3, Figure 5 & 6**).

444 The most severe *ndh* gene loss occurred in the plastome of *D. variegatum*, with *ndhA*, *ndhB*,
445 *ndhD* and *ndhK* severely pseudogenised and *ndhJ* moderately pseudogenised.

446 The greatest degradation processes within *Dipodium* occurred for the *ndhG* gene, which was
447 putatively lost in almost all plastomes, except *D. stenocheilum* 1 which retained a severely
448 pseudogenised *ndhG* gene (**Figure 6**). This was followed by *ndhK*, which was lost in 19 out of
449 24 plastomes (*D. ensifolium*, *D. hamiltonianum*, *D. interaneum*, the *D. roseum* complex and
450 the *D. stenocheilum* complex) (**Figure 6**). In the six remaining plastomes *ndhK* was conserved
451 to different degrees. *D. punctatum*, *D. pulchellum* and *D. campanulatum* 2 retained more than
452 90% of the homologous bases compared to the functional *ndhK* gene of *M. coccinea*
453 (KP205432, Kim et al., 2015) but showed severe frameshift mutations and indels which caused
454 several internal stop codons. The plastomes with severely pseudogenised *ndhK* genes exhibited
455 large truncations.

456 Nine *Dipodium* samples (*D. ammolithum*, *D. atropurpureum* 1, *D. elegantulum*, *D. pardalinum*
457 1, *D. roseum* 1 & 2, *D. aff. roseum* 2, *D. stenocheilum* 2, and *D. variegatum*) putatively lost
458 the *ndhC* gene. In *D. punctatum* *ndhC* was moderately pseudogenised and in the remaining
459 plastomes *ndhC* was severely pseudogenised (**Figure 6**). Only *D. ensifolium* showed an intact
460 start codon for the *ndhC* gene but suffered a severe truncation with the loss of ca. 50% of
461 homologous bases compared to the functional *ndhC* gene of *M. coccinea* (KP205432, Kim et
462 al., 2015).



463

464 **Figure 6:** Pattern of putative *ndh* gene degradation in *Dipodium*. Gene degradation plotted against the
 465 maximum likelihood tree with focus on 24 fully assembled plastomes. (outgroups not shown). Support
 466 values (SHaLRT/ UFboot) are shown on each branch. ps = pseudogenisation; *D. ham.* = *D.*
 467 *hamiltonianum*

468

469 In *D. pandanum* 1, *D. stenocheilum* 1, and *D. variegatum* the *ndhF* gene was putatively lost
 470 (**Figure 6**). All other samples possessed severely truncated *ndhF* genes with absent start codons
 471 and multiple internal stop codons. The *ndhH* gene was present in *D. pandanum* 1 possessing a
 472 length of 1,176 bp (99.2% of homologous length compared to *M. coccinea* (KP205432, Kim
 473 et al., 2015). In most other samples, the *ndhH* gene was degraded possessing several stop
 474 codons. *D. stenocheilum* 1 and *D. variegatum* lost the *ndhH* gene (**Figure 5**, **Figure 6**).

475 Moreover, *ndhE*, *ndhI* and *ndhA* were found to be putatively lost in the plastome of *D.*
476 *variegatum* and *D. pandanum* 1, respectively (**Figure 5**, **Figure 6**). No gene loss occurred for
477 *ndhB*, *ndhD* and *ndhJ*, however all three genes exhibited various degrees of degradation within
478 all examined *Dipodium* plastomes and were either moderately or severely pseudogenised due
479 to internal stop codons or frame-shift mutations.

480 The *ndhD* gene was found to have undergone the fewest degradation processes in regards of
481 gene length which was largely conserved ranging from 1,122 bp (*D. campanulatum* 1) to 1,521
482 bp (*D. pulchellum*) and in most plastomes *ndhD* possessed the alternative start codon ACG
483 (Threonine). Furthermore, almost all *Dipodium* plastomes showed the canonical AUG
484 (Methionine) start codon for *ndhA*, *ndhB*, *ndhE*, and *ndhI*. The intron-containing *ndhA* and
485 *ndhB* genes exhibited the strongest degradation (i.e., large deletions) within the intron regions
486 and the downstream exon in all *Dipodium* samples. Exon1 of *ndhB* was almost complete and
487 in-frame for most plastomes and showed only one point mutation (from A to C) which resulted
488 in a stop codon at amino acid position 68 (after 201 bp from the beginning of the first exon in
489 *ndhB*).

490 Within different *Dipodium* complexes the patterns for putative *ndh* gene losses and severe or
491 moderate pseudogenisations were similar for examined plastomes of *D. hamiltonianum* and *D.*
492 *interaneum*. Both plastomes putatively lost *ndhG* and *ndhK* and showed severe
493 pseudogenisations of *ndhA*, *ndhB*, *ndhC*, *ndhF*, *ndhH*, *ndhJ* and a moderately pseudogenised
494 *ndhE* gene, but differed in level of putative pseudogenisation of *ndhD* and *ndhI* (**Figure 6**).

495 Other similarities were found in the *D. roseum* complex, in which the *ndhD* gene was
496 moderately pseudogenised in all samples. Almost all samples of the *D. roseum* complex, except
497 for *D. roseum* 2, harboured moderately pseudogenised *ndhE* and *ndhI* genes.

498 Within the same species, only *D. aff. roseum* 3 and *D. aff. roseum* 4 showed the same pattern
499 of *ndh* gene loss and level of degradation which was also present in the plastome of *D.*
500 *pardalinum* 2. Within the *D. stenocheilum* complex, *D. stenocheilum* 1 putatively lost *ndhI* and
501 *ndhF*.

502 Across other samples, only two plastome pairs (*D. ensifolium* and *D. aff. roseum* 1; *D.*
503 *basalticum*, and *D. atropurpureum* 2) shared the same pattern of *ndh* gene loss and degradation.
504 In comparison to all other species of examined *Dipodium* plastomes, *D. variegatum*
505 independently lost *ndhE* and *ndhI* and *D. pandanum* 1 lost the *ndhA* gene (**Figure 6**).

506
507

508 4 Discussion

509 This is the first molecular study to elucidate interspecific relationships and divergence times in
510 *Dipodium* and to examine plastid genome degradation within a mycoheterotrophic orchid
511 genus of the Australasian flora in a phylogenomic context.

512 4.1 Phylogenetic placement and infrageneric relationships of *Dipodium*

513 This phylogenomic study based on 68 plastid loci provided strong support for the monophyly
514 of *Dipodium* and its phylogenetic placement as an early diverging lineage within tribe
515 Cymbidieae. Previous phylogenetic studies included only one or two species of *Dipodium*
516 which precluded assessment of the monophyly of the genus (Pridgeon et al., 2009; Chase et
517 al., 2015; Górnjak et al. (2010); Batista et al. (2014); Freudenstein and Chase (2015); Kim et
518 al., 2020; Serna-Sánchez et al., 2021; McLay et al., 2023; Pérez-Escobar et al., 2023). Our
519 study resolved *Dipodium* as the diverging early within Cymbidieae after subtribe Cymbidiinae
520 with strong support and thus confirmed previous molecular phylogenetic studies in support of
521 recognition of *Dipodium* at subtribal level as Dipodiinae (Li et al., 2016; Serna-Sánchez et al.,
522 2021; Kim et al., 2020; Pérez-Escobar et al., 2023).

523 This phylogenomic study present the first molecular evidence in support of the infrageneric
524 classification of *Dipodium* into sect. *Dipodium* and sect. *Leopardanthus* (O'Byrne, 2014;
525 O'Byrne, 2017; Jones, 2021), lending support to the diagnostic value of vegetative traits (i.e.,
526 the presence or absence of adventitious roots) in infrageneric classification of *Dipodium*.
527 Section *Leopardanthus* is characterised by leafy species which possess adventitious roots, such
528 as *Dipodium pandanum*. In contrast, sect. *Dipodium* comprises species without adventitious
529 roots and includes all leafless species, the leafy species *D. ensifolium*, and the morphologically
530 similar *D. gracile* from Sulawesi, the latter being only known from the type (destroyed)
531 (O'Byrne, 2017). Our phylogenomic study supported the placement of the *D. ensifolium* in
532 sect. *Dipodium*, resolved as sister to all leafless species in the section. However, further
533 molecular study is warranted to ascertain the monophyly of the two sections based on an
534 expanded sampling of sect. *Leopardanthus*.

535 Our phylogenomic study is the first to shed light on evolutionary relationships within sect.
536 *Dipodium*, which was found to comprise six main lineages. The phylogenomic framework now
537 allows assessment of useful diagnostic morphological traits to characterise main lineages
538 within the section. For example, the yellow stem and flower colour of species of the *D.*
539 *hamiltonianum* complex easily distinguishes this clade from other mycoheterotrophic orchids

540 within sect. *Dipodium* (**Figure 1**; Jones, 2021). Stems of remaining mycoheterotrophic species
541 of sect. *Dipodium* are mostly greenish to dark reddish or purplish, whereas flowers vary in
542 color from pale white, pinkish to purplish (**Figure 1**, Barrett et al., 2022; Jones, 2021). Also,
543 sepal and petal characters were found to differ among clades: for example, species of clade A,
544 comprising the *D. hamiltonianum* and *D. stenocheilum* complexes, possess sepals and lateral
545 petals that are markedly narrower compared to species of clade B (comprising the *D. punctatum*
546 and *D. roseum* complex) and *D. ensifolium*, the first diverging lineage within the sect.
547 *Dipodium* (**Figure 1**; **Figure 3**) (Barrett et al., 2022; Jones, 2021).

548 Phylogenetic divergence within the two species complexes in clade B, *i.e.*, the *D. punctatum*
549 and the *D. roseum* complexes, was shallow overall and thus interspecific relationships in these
550 two groups remained largely unclear (**Figure 3**). Previous morphological studies highlighted
551 difficulties in species delimitation within the *D. punctatum* complex, in particular between *D.*
552 *pulchellum* and *D. punctatum* (Jones, 2021). While *D. pulchellum* is morphologically very
553 similar to *D. punctatum*, the two species are differentiated by the intensity of their flower
554 colours, which are richer in *D. pulchellum* and paler in *D. punctatum* (Jones and Clements,
555 1987). However, a morphological study by Jones (2021) revealed that the strong floral
556 coloration of *D. pulchellum* flowers was likely due to differences in environmental factors (*i.e.*,
557 soil type and rainfall regime) of growing sites and thus Jones (2021) proposed to synonymise
558 *D. pulchellum* with *D. punctatum*.

559 Similar challenges in taxonomic delimitation based on flower colours are also evident within
560 the *D. roseum* complex. The distribution of the more widespread species *D. roseum* largely
561 overlaps with the distributions of *D. atropurpureum* and *D. pardalinum* (ALA, 2023). Besides
562 a very similar growing habit, the flowers of the three species are very similar in shape and vary
563 only slightly in coloration: *D. roseum* has bright, rosy flowers with small darker spots, *D.*
564 *atropurpureum* possesses dark pinkish-purple to dark reddish-purple flowers with spots and
565 blotches, and the flowers of *D. pardalinum* are pale pink to white with large reddish spots and
566 blotches (**Figure 1**) (Jones, 2021). Taken together, the overlapping distribution, similar
567 appearance, and very shallow genetic divergence found in the present study among species in
568 the *D. roseum* complex suggest that *D. atropurpureum* and *D. pardalinum* may be colour
569 variations of *D. roseum*. Further molecular study with more highly resolving molecular
570 techniques such as genotyping-by-sequencing is required to rigorously assess species
571 delimitation within *Dipodium*.

572

573 4.2 Divergence-time estimations

574 Our divergence time estimations yielded results comparable to previous studies regarding the
575 temporal diversification of major orchid clades (e.g., Givnish et al., 2015, Givnish et al., 2018;
576 Kim et al., 2020; Serna-Sánchez et al., 2021; Zhang et al., 2023). Within Epidendroideae, this
577 study confirmed that Cymbidieae was one of the most recently diverged tribes in Orchidaceae,
578 consistent with previous studies (e.g., Givnish et al., 2015; Serna-Sánchez et al., 2021; Zhang
579 et al., 2023). Stem and crown diversification of Cymbidieae were estimated to have
580 commenced at ca. 42.2 Ma and 38.0 Ma respectively, which is similar to the estimates of Serna-
581 Sánchez et al. (2021) and slightly younger than those of Zhang et al. (2023) (**Figure 4**,
582 Supplementary Material 4 and 5).

583 Our study is the first to elucidate phylogenetic relationships and divergence times within
584 *Dipodium*. Previously, only two studies included a representative of *Dipodium* (*D. roseum*,
585 MN200368) in divergence-time estimations for Orchidaceae (Kim et al., 2020; Serna-Sánchez
586 et al., 2021). These studies estimated the origin of *Dipodium* to ca. 17 Ma and ca. 31 Ma,
587 respectively. Our study placed the divergence of *Dipodium* from the other subtribes in
588 Cymbidieae to ca. 33.3 Ma in the early Oligocene which is closer to the findings of Serna-
589 Sanchez et al. (2021). O’Byrne (2014) hypothesised that lineage divergence into sect.
590 *Dipodium* and sect. *Leopardanthus* resulted from vicariance in conjunction with the break-up
591 of Pangaea, in particular the separation of the Indian and Australian continental plates
592 (O’Byrne, 2014). However, our divergence-time estimations show that *Dipodium* is far too
593 young (< 33 Ma) to have been influenced by the break-up of Pangaea, which occurred from
594 the early Jurassic and onwards. Lineage divergence of sect. *Dipodium* and sect. *Leopardanthus*
595 were estimated to ca. 11.3 Ma in the late Miocene (**Figure 4**), when Australia had already
596 assumed, approximately, its present geographical position. Rather, *Dipodium* is likely to have
597 achieved its current distribution through range expansion between Australia and Southeast Asia
598 across the Sunda-Sahul Convergence Zone (Joyce et al. 2021a), consistent with a general
599 pattern of floristic exchange – the Sunda-Sahul Floristic Exchange - which was initiated as
600 early as c. 30 Ma (Crayn et al., 2015; Joyce et al., 2021b). However, the data are insufficient
601 at present to resolve the ancestral area of *Dipodium* and its main lineages. Further research is
602 needed including an increased sampling to shed light on range evolution of *Dipodium* through
603 ancestral range reconstruction.

604 Our results indicate that the Australian leafy species *D. ensifolium* diverged from the remainder
605 of section *Dipodium* approximately 8.1 Ma (late Miocene) (**Figure 4**). The remainder of the

606 sect. *Dipodium* clade, which includes all leafless, putatively fully mycoheterotrophic species,
607 emerged ca. 7.3 Ma (late Miocene) followed by rapid diversification from ca. 4.3 Ma onwards
608 (early Pliocene) (**Figure 4**). Thus, mycoheterotrophy has most likely evolved only once within
609 *Dipodium*, on the Australian continent during the late Miocene-early Pliocene.

610 From the late Miocene-early Pliocene (ca. 5 Ma) climatic conditions in Australia became
611 increasingly arid, leading to a decline of rainforest vegetation and expansion of open
612 sclerophyllous forests (Quilty, 1994, Gallagher et al., 2003, Martin, 2006, He and Wang, 2021).
613 By the end of the Pliocene Australia's landscape was similar to the present day, with much of
614 the continent a mosaic of open woody vegetation dominated by *Eucalyptus*, *Acacia* and
615 Casuarinaceae (e.g., Martin 2006). The Pleistocene (ca. 2.58 – 0.012 Ma) was characterised by
616 climatic oscillations which led to repeated forest expansion and contraction (Byrne, 2008). The
617 evolution of mycoheterotrophy and the subsequent radiation of sect. *Dipodium* may have been
618 facilitated by two factors: aridification in Australia favouring the reduction of leaf area to
619 decrease water loss (O'Byrne, 2014), and the expansion of sclerophyll taxa and their
620 mycorrhizal partners. Mycoheterotrophic *Dipodium* are assumed to share mycorrhizal fungi
621 with Myrtaceae trees, especially *Eucalyptus*, (Bougoure and Dearnaley, 2005; Dearnaley and
622 Le Brocque, 2006; Jones, 2021) which explosively diversified and came to dominate most
623 Australian forests and presumably led to an increased diversity and abundance of suitable
624 mycorrhizal partners for *Dipodium*. The rapid diversification of *Dipodium* from the Pleistocene
625 onwards (ca. 3.2–0.3 Ma) (**Figure 4**) may have been driven by cycles of population
626 fragmentation and coalescence in response to climatic oscillations.

627 **4.3 Plastid genome evolution**

628 **4.3.1 Plastome structural features and variations**

629 In this study, whole plastome assemblies were generated for 24 *Dipodium* samples, including
630 representatives of all leafless, putatively full mycoheterotrophs of sect. *Dipodium* found in
631 Australia, one leafy photosynthetic species of sect. *Dipodium* (*D. ensifolium*) and one leafy
632 photosynthetic species of sect. *Leopardanthus* (*D. pandanum*). The overall organisation and
633 the plastid gene content is generally conserved in most examined *Dipodium* plastomes (**Figure**
634 **5, Table 2 and 3**). All examined plastomes showed the typical quadripartite structure of
635 angiosperms (Ruhlman and Jansen 2014). However, some genomic features among several
636 *Dipodium* plastomes were not conserved, including 1) differences in total genome length; 2)
637 independent boundary shift IRB/SSC/IRA within the plastome of *D. pandanum* 1, *D.*
638 *stenocheilum* 1, *D. variegatum*; 3) triplication of the *trnV*-GAC in the plastomes of *D.*

639 *ammolithum*, *D. elegantulum*, *D. hamiltonianum*, *D. stenocheilum* 2, *D. interaneum* 4) the
640 independent pseudogenisation of *cemA* in the plastome of *D. aff. roseum* 4 and *trnD-GUC* in
641 the plastome of *D. campanulatum* 1; and 5) the pseudogenisation or loss to varying degrees of
642 *ndh* genes (**Figure 5**, **Table 3**, Supplementary Material 7).

643 Total genome length of *Dipodium* plastomes displayed differences of around 10,000 bp
644 between the smallest (142,949 bp; *Dipodium variegatum*) and largest plastomes (152,956 bp
645 *Dipodium aff. roseum* 3) which correlated with level of *ndh* gene degradation. Some *Dipodium*
646 plastomes were similar to the average size of orchid plastomes (152,442 bp) published on NCBI
647 database (286 Orchidaceae chloroplast genome, accessed on June 13, 2022), however most
648 plastomes were smaller (average size *Dipodium* plastomes: 148,703 bp; **Table 2**). Average GC
649 contents in *Dipodium* was very similar to the average GC content of published orchid plastomes
650 on NCBI database (ca. 36.8%; 286 Orchidaceae chloroplast genome, accessed on June 13,
651 2022) and all fell into the range of typical angiosperm plastomes (ca. 30–40%) (**Table 2**).

652 **4.3.2 Patterns of *ndh* gene degradation within *Dipodium***

653 In orchids, *ndh* gene losses and pseudogenisations which occurred in both autotrophic and
654 heterotrophic species have been documented in various genera (e.g., Kim et al., 2015; Feng et
655 al., 2016; Niu et al., 2017; Barrett et al., 2018, Barrett et al., 2019; Roma et al., 2018; Lallemand
656 et al., 2019; Kim et al., 2020; Peng et al., 2022; Kim et al., 2023). This study is in line with
657 these general findings in that *ndh* gene degradation was also observed within the orchid genus
658 *Dipodium*. All chloroplast *ndh* genes in *Dipodium* plastomes exhibited varying degrees of
659 putative pseudogenisation and loss, not a single *ndh* gene remained functional among the
660 examined chloroplast genomes (**Table 3**, **Figure 5**, **Figure 6**). These findings include all
661 plastomes of leafless putatively fully mycoheterotrophic species and of two autotrophic leafy
662 species (*D. pandanum* and *D. ensifolium*) and thus suggest that all examined species,
663 independently of their nutritional status, have lost the functionality of the plastid NADH
664 dehydrogenase complex. Hence, the last common ancestor of extant *Dipodium* is likely to have
665 lacked a functional NDH complex. Previous studies in Cymbidiinae, the first diverging lineage
666 in Cymbidieae, found that all species studied so far exhibited at least one degraded *ndh* gene
667 (e.g., Yang et al., 2013; Kim and Chase 2017). As the next diverging lineage in Cymbidieae is
668 *Dipodium*, this suggests that the degradation of *ndh* genes in Cymbidieae was likely a dynamic
669 process from functional to non-functional. However, further research is needed e.g., ancestral
670 state reconstructions of gene degradation with increased taxonomic sampling. The inclusion of

671 more species among sect. *Leopardanthus* is warranted to clarify if some *ndh* genes have
672 remained functional in some autotrophic species of sect. *Leopardanthus*.

673 Previous studies examined *ndh* gene loss at genus level and revealed an independent loss of
674 function of the NADH dehydrogenase complex for several genera (e.g., Lin et al., 2015, Kim
675 et al., 2015). However, comparative whole plastome studies examining gene degradation and
676 loss among closely related mycoheterotrophic species are still scarce. For a better
677 understanding of *ndh* gene degradation patterns this study investigated the degree of *ndh* gene
678 degradation among closely related orchid species (**Figure 6**). Greatest degradation within
679 *Dipodium* were found for *ndhG* which is putatively lost in almost all examined plastomes,
680 except *D. stenocheilum* 1 which retained a putative severely pseudogenised *ndhG* (**Figure 6**).
681 The *ndhG* gene is located within the SSC region. In general, it is well established that genes in
682 the SSC region experience higher substitution rates compared to genes located within IR
683 regions (Ruhlman and Jansen 2014). The latter is the case for *ndhB* which is located in the IRs
684 and structurally more conserved in *Dipodium* compared to most *ndh* genes located in the SSC.
685 The greatest degree of *ndh* gene degradation occurred in *D. variegatum* which putatively lost
686 *ndhC* and *ndhE–ndhI*. All other plastomes putatively lost at least one to three *ndh* genes and
687 showed different levels of degradation (**Figure 6**).

688 Interestingly, the level of *ndh* gene degradation varied even among closely related species
689 within species complexes. For example, *D. stenocheilum* 1 independently lost *ndhI* and *ndhF*,
690 whereas all other studied samples of the *D. stenocheilum* complex retained those two genes as
691 moderately or severely pseudogenised (**Figure 6**). Different levels of gene degradation and loss
692 were even found within the same species. For example, *D. atropurpureum* 1 lost *ndhC* whereas
693 *D. atropurpureum* 2 retained a severely pseudogenised *ndhC* (**Figure 6**). Moreover, the study
694 of Kim et al., (2020) included one individual of *D. roseum* which showed a different pattern of
695 *ndh* gene loss and degradation to those found among the *D. roseum* samples of this study. *D.*
696 *roseum* (MN200386) experienced complete loss of *ndhA*, *ndhC–ndhI* and *ndhK*, but retained
697 pseudogenised *ndhB* and *ndhJ* genes (Kim et al., 2020). These findings also agree with the
698 recent comparative plastome study on *D. roseum* and *D. ensifolium*: *D. roseum* (OQ885084)
699 has retained truncated *ndhB*, *ndhD* and *ndhJ* genes, but completely lost *ndhA*, *ndhC*, *ndhE–*
700 *ndhI* and *ndhK* (McLay et al., 2023).

701 Overall, some patterns of *ndh* gene degradation found in this study in *Dipodium* are similar,
702 however many were unique for each individual examined. Hence, this suggests that sect.
703 *Dipodium* has undergone a recent and active *ndh* gene degradation which strongly implies a
704 relaxed evolutionary selective pressure for the retention of the NDH complex.

705 4.3.3 IR/SSC junctions and IR instability

706 Orchidaceae plastomes frequently show an expansion/shift of the IR towards the SSC region
707 (e.g., Kim et al., 2020). This instability of the IR/SSC junction is assumed to correlate with the
708 deletion of *ndhF* and has resulted in a reduction of the SSC, as observed in several Orchidaceae
709 plastomes (e.g., Kim et al., 2015; Niu et al., 2017; Dong et al., 2018; Roma et al., 2018) and in
710 other land plant plastomes (e.g., Amaryllidaceae, Bignoniaceae, Orobanchaceae) (Thode and
711 Lohmann 2019; Li et al., 2021; Könyves et al., 2021). This study revealed reduced SSC regions
712 for most examined plastomes which correlated with the degradation of the *ndh* gene suite
713 located in the SSC. Compared to typical SSC regions found in angiosperms (ca. 20 kb,
714 Ruhlman and Jansen 2014), the smallest SSC region was reduced by ca. 7,900 bp (*D.*
715 *variegatum*) and the largest SSC region was reduced by ca. 4,700 bp (*D. ensifolium*) (**Table 2**,
716 **Figure 5**). However, a large expansion of the IR such as found in *Vanilla* and *Paphiopedilum*
717 plastomes (Kim et al., 2015) was not found in *Dipodium* (IR sizes ranging between 24,436–
718 26,817 bp, **Table 2**).

719 In angiosperms, the *ycf1* gene usually occupies ca. 1,000 bp in the IR (Sun et al., 2017, Kim et
720 al., 2015). *Dipodium* plastomes in this study displayed varying positions of *ycf1* within the IR.
721 In plastomes in which the *ndhF* gene was completely lost or severely truncated, the portion of
722 *ycf1* within the IRA was mostly shorter compared to plastomes which contained moderately
723 truncated *ndhF* genes (**Figure 5**). These results are similar with findings of Kim et al., (2015),
724 a study which compared the locations of the IR/single-copy region junctions among 37 orchid
725 plastomes and closely related taxa in Asparagales. In at least three plastomes (*D. pandanum* 1,
726 *D. stenocheilum* 1, *D. variegatum*) *ndhF* was independently lost, the SSC/IRB junction was
727 shifted into the spacer region near the *rpl32* gene in direct adjacency to the partially duplicated
728 *ycf1* fragment (**Figure 5**, D, b–d). These findings suggest the deletion of *ndhF* correlated with
729 the shift of the SSC/IRB junction. Interestingly, the boundaries between SSC and IR regions
730 were found to be variable even among closely related species e.g., in *Cymbidium*. Some species
731 in *Cymbidium* showed similar patterns of IR/SSC shifts (Kim and Chase 2017) as found in
732 *Dipodium*.

733 In at least five plastomes (*D. ammolithum*, *D. elegantulum*, *D. hamiltonianum*, *D. interaneum*,
734 *D. stenocheilum* 2) the *trnV*-GAC gene was triplicated (i.e., duplicated *trnV*-GAC version in
735 close proximity to each other either in IRA or IRB) (**Figure 5**, B, C; **Table 3**). To the best of
736 our knowledge, similar tRNA duplication patterns within the IR regions have not yet been
737 found in any other Orchidaceae plastome. However, a recent study on plastomes of the
738 angiosperm genus *Medicago* (Wu et al., 2021) yielded similar patterns. Wu et al. (2021) have

739 found three copies of the *trnV*-GAC gene in the plastomes of two closely related species within
740 the IR (*M. archiducis-nicolai* and *M. ruthenica*) which were linked to forward and tandem
741 repeats. Interestingly, Wu et al. (2021) findings support the hypothesis that repetitive sequences
742 lead to genomic rearrangements and thus affect plastome stability. This may also apply for
743 some *Dipodium* plastomes. However, to rule out any technical issues throughout the NGS
744 process and to validate findings of duplicated tRNAs (and above-mentioned boundaries of
745 IR/SC regions), PCR amplification of affected regions should be carried out in future studies.
746 However, in strong support of tRNA duplication is their independent presence within the IR of
747 five plastomes among individuals of the same species complexes (*D. stenocheilum* complex
748 and *D. hamiltonianum* complex). However, an increased sampling is necessary to better
749 understand the impacts of genomic rearrangements due to repetitive sequences and thus
750 plastome instability in *Dipodium*.

751 **4.3.4 Evolution of mycoheterotrophy and associated plastome degradation in** 752 ***Dipodium***

753 Heterotrophic plants are remarkable survivors, exhibiting often curious morphological,
754 physical, or genomic modifications. Multiple heterotrophs were found to have suffered plastid
755 genome degradations due to relaxed pressure on photosynthetic function. In recent years,
756 evidence has accumulated that plastid genomes have undergone gene degradation in the
757 evolutionary transition from autotrophy to heterotrophy (e.g., Graham et al., 2017; Barrett et
758 al., 2019; Wicke et al., 2016). Among these, the first stage is the loss and pseudogenisation of
759 genes involved in encoding the NDH complex. Interestingly, all examined plastomes of
760 *Dipodium* have lost or pseudogenised all 11 *ndh* genes regardless of their nutritional status
761 (**Figure 6**). Two photosynthetic species with green leaves were included in this study, *D.*
762 *pandanum* (sect. *Leopardanthus*) and *D. ensifolium* (sect. *Dipodium*). Degradation in *ndh*
763 genes among photosynthetic species is not surprising and was frequently reported in previous
764 plastome studies in land plants. The large-scale study on Orchidaceae plastomes of Kim et al.,
765 (2020) observed *ndh* gene pseudogenisation and losses among species in many epiphytes and
766 several terrestrials which have retained their photosynthetic capacity. The NDH complex is
767 thought to mediate the Photosystem I cyclic electron transport, fine-tunes photosynthetic
768 processes and alleviates photooxidative stress (e.g., Yamori et al., 2015; Peltier et al., 2016;
769 Sabater 2021). *D. pandanum* is a terrestrial or climbing epiphytic orchid and highly localised
770 in rainforest habitats, whereas the terrestrial *D. ensifolium* grows in open forests and woodlands
771 (Jones, 2021), thus both species seem to prefer shaded understory habitats. For epiphytic or
772 terrestrial plants living in low-light habitats it has been proposed that the NDH complex may

773 not be essential anymore (e.g., Barrett et al., 2019). One reason for this may be that they are
774 less exposed to photooxidative stress (e.g., Feng et al., 2016; Barrett et al., 2019). However,
775 the NDH complex is composed of 11 chloroplast encoded subunits and additional subunits
776 encoded by the nucleus (e.g., Peltier et al., 2016). It has been established that genomic material
777 was repeatedly exchanged between the nucleus, mitochondrion, and chloroplast in the
778 evolutionary course of endosymbiosis. Thus, previous studies examined whether genes were
779 transferred from the chloroplast to the nucleus and/or mitochondrion genome or whether
780 nuclear genes for the NDH complex suffered under degradation. Indeed, Lin et al., (2015)
781 reported *ndh* fragments within the mitochondrial genomes of orchids, however no copies were
782 found in the nuclear orchid genomes. Similar findings were reported from the orchid genus
783 *Cymbidium* (Kim and Chase et al., 2017). However, further studies are needed to determine
784 whether *ndh* gene transfer into the nucleus or mitochondrion may play a role within *Dipodium*.
785 The proposed subsequent next steps toward (myco-) heterotrophy is the functional loss of
786 photosynthetic genes (e.g., *psa*, *psb*, *pet*, *rbcL* or *rpo*) followed by genes for the chloroplast
787 ATP synthase and genes with other function such as housekeeping genes (e.g., *matK*, *rpl*, *rnn*
788 (e.g., Graham et al., 2017; Barrett et al., 2019). Most examined *Dipodium* plastomes displayed
789 no additional plastid gene degradation besides *ndh* gene degradation, except in *D. aff. roseum*
790 4 where *cemA* was pseudogenised and in *D. campanulatum* 1 where the *trnD-GUC* gene was
791 pseudogenised (**Table 3**). The *cemA* gene encodes the chloroplast envelope membrane protein
792 and was found to be non-essential for photosynthesis, however *cemA*-lacking mutants of the
793 green alga *Chlamydomonas* were found to have a severely affected carbon uptake (Rolland et
794 al., 1997) and may therefore be classified as directly involved in photosynthesis. Transfer RNA
795 genes (*trn*) are involved in the translation process and categorised as ‘housekeeping’ genes
796 (e.g., Graham et al., 2017; Wicke and Naumann 2018; Barrett et al., 2019). Moreover, similar
797 gene degradation patterns were found in the plastomes of *D. roseum* (MN200386, Kim et al.,
798 2020 and OQ885084, Mclay et al., 2023) and *D. ensifolium* (OQ885084, Mclay et al., 2023),
799 which functionally lost all *ndh* genes. However, most photosynthesis related genes in the
800 plastomes of *Dipodium* were found to be functional. Thus, mycoheterotrophic species of
801 *Dipodium* display evidence of being at the beginning of plastid gene degradation, in contrast
802 with the majority of fully mycoheterotrophic orchids which are in more advanced stages of
803 degradation, e.g. *Cyrtosia septentrionalis* (Kim et al., 2019), *Epipogium* (Schelkunov et al.,
804 2015), and *Rhizanthella* (Delannoy et al., 2011). On the other hand, mycoheterotrophs such as
805 *Corallorhiza trifida* (Barrett et al., 2018), *Cymbidium macrorhizon* (Kim et al., 2017),
806 *Hexalectris grandiflora* (Barrett et al., 2019) and *Limodorum abortivum* (Lallemand et al.,

807 2019) display functionally losses within the plastid *ndh* genes only and some species among
808 them additionally lost one or two other genes, similar to findings in *Dipodium*. Interestingly,
809 most of these species are leafless, but considered putatively partially mycoheterotrophic.
810 Suetsugu et al. (2018) demonstrated that the leafless green orchid *Cymbidium macrorhizon*
811 contains chlorophyll and can fix significant quantities of carbon during the fruit and seed
812 production phase and thus, is photosynthetically active. Chlorophyll is present in *Corallorhiza*
813 *trifida* also, but this green, leafless coralroot is an inefficient photosynthesiser (Barrett et al.,
814 2014). Some species among leafless orchids within sect. *Dipodium* (e.g., *D. elegantulum*, *D.*
815 *stenocheilum*, *D. variegatum*) appear green on stems (**Figure 1**, Jones 2021), which suggests
816 they may contain some chlorophyll and be able to photosynthesise. Coupled with relatively
817 mild plastid gene degradation compared to other fully mycoheterotrophic orchids, this suggests
818 some leafless species among sect. *Dipodium* may be partially mycoheterotrophic rather than
819 fully mycoheterotrophic as has been hypothesised for *D. roseum* (Kim et al. 2020; McLay et
820 al. 2023). However, no studies so far have examined whether leafless species among sect.
821 *Dipodium* contain chlorophyll and whether they are capable to carry out photosynthesis at
822 sufficient rates. Therefore, more research is needed to assess the trophic status, including
823 analysis of chlorophyll quantities and the ratio of photosynthetic carbon to fungal carbon for
824 *Dipodium*.

825 Compared with recently published studies on mycoheterotrophic orchids such as *Corallorhiza*
826 and *Hexalectris* (Barret et al. 2018; Barret et al. 2019) which incorporated divergence time
827 estimations, plastomes of *Dipodium* showed the least degradation. *Hexalectris* crown age was
828 estimated to ca. 24 Ma and plastomes of mycoheterotrophs were more degraded compared to
829 mycoheterotrophic plastomes of *Corallorhiza* which diversified ca. 9 Ma onwards (Barret et
830 al. 2018; Barret et al. 2019). *Dipodium* diversified in the late Miocene ca. 11 Ma, and the
831 mycoheterotrophic lineage divergent from the autotrophic lineage ca. 8.1 Ma which is slightly
832 younger compared to *Corallorhiza*. Hence, time of divergence may play a role in the degree of
833 degradation of *Dipodium* plastomes which show an early stage of plastome degradation
834 compared to older diverging mycoheterotrophic lineages that are in more advanced stages of
835 plastome degradation.

836 **5 Conclusion**

837 This molecular phylogenomic comparative study clarified evolutionary relationships and
838 divergence times of the genus *Dipodium* and provided support for two main lineages within

839 *Dipodium*, corresponding to the morphologically defined sect. *Dipodium* and sect.
840 *Leopardanthus*. Phylogenetic analysis resolved the leafy autotroph *D. ensifolium* as being part
841 of sect. *Dipodium* and found to be in sister group position to all leafless species in sect.
842 *Dipodium*. Divergence-time estimations placed the divergence of the leafy species *D.*
843 *ensifolium* from the remainder of section *Dipodium* in the late Miocene. Shortly after, the
844 remaining clade including all leafless, putatively full mycoheterotrophic species within sect.
845 *Dipodium* emerged ca. 7.3 Ma in the late Miocene followed by rapid species diversification
846 from ca. 4.3 Ma onwards in the early Pliocene. Thus, this study indicates that
847 mycoheterotrophy has most likely evolved only once on the Australian continent within
848 *Dipodium* during the late Miocene, and that the ancestors of putatively full mycoheterotrophic
849 species may have had green leaves. Among the examined plastomes, all plastid *ndh* genes were
850 pseudogenised or physically lost, regardless of the individual's nutrition strategy (i.e.,
851 autotroph versus mycoheterotroph). Thus, this study provides molecular evidence of relaxed
852 evolutionary selective pressure on the retention of the NADH dehydrogenase complex.
853 Mycoheterotrophic species among sect. *Dipodium* retained a full set of other functional
854 photosynthesis-related genes and exhibited an early stage of plastid genome degradation.
855 Hence, leafless species of sect. *Dipodium* may potentially be rather partially mycoheterotrophic
856 than fully mycoheterotrophic.

857 To further disentangle evolutionary relationships in *Dipodium*, future studies based on nuclear
858 data such as derived from target capture sequencing and with a denser sampling at population
859 level are warranted. Moreover, the inclusion of a denser sampling of sect. *Leopardanthus* is
860 warranted to clarify if some *ndh* genes may have remained functional in some of the autotrophic
861 species of sect. *Leopardanthus*. To obtain further insights into the nutritional strategies in
862 *Dipodium*, future studies should assess the trophic status of mycoheterotrophic species in
863 *Dipodium* based on physiological data such as from the analysis of chlorophyll quantities and
864 the ratio of photosynthetic carbon to fungal carbon for *Dipodium*. The Australian orchid flora
865 harbours many more remarkable mycoheterotrophic lineages (e.g., *Danhatchia*) which offer
866 the opportunity to further explore the evolutionary pathways to mycoheterotrophy and
867 associated plastid genome evolution. The inclusion of autotrophic plants into comprehensive
868 plastid phylogenetic analyses could broaden the understanding of the significance of observed
869 *ndh* gene degradation patterns within Orchidaceae.

Tables

Table 1. Plant material used in this study inclusive voucher details and provenances with botanical districts. Taxonomy according to the Australian Plant Census (APC, 2023). CANB = Australian National Herbarium, CNS = Australian Tropical Herbarium. AU = Australia, PG= Papua New Guinea. ACT = Australian Capital Territory, NT = Northern Territory, NSW = New South Wales, SA = South Australia, QLD = Queensland, WA = Western Australia, Vic = Victoria.

Species	DNA extract No.	Voucher details	Provenance
<i>Dipodium</i> aff. <i>roseum</i> 1	HTCG 0828	C. Bower ORG7817 (CANB 906470.1)	AU: NSW; Central Tablelands; Mullions Range State Forest
<i>Dipodium</i> aff. <i>roseum</i> 2	HTCG 0830	C. Bower ORG7818 WP 6 (CANB 906471.1)	AU: NSW; Central Tablelands; Mount Canobolas State Conservation Area
<i>Dipodium</i> aff. <i>roseum</i> 3	HTCG 0831	C. Bower ORG7818 WP 7 (CANB 906471.1)	AU: NSW; Central Tablelands; Mount Canobolas State Conservation Area
<i>Dipodium</i> aff. <i>roseum</i> 4	HTCG 0832	C. Bower ORG7818 WP 9,10,11 (CANB 906471.1)	AU: NSW; Central Tablelands; Mount Canobolas State Conservation Area
<i>Dipodium</i> aff. <i>stenocheilum</i>	HTCG 1691	D.L. Jones 8968 (CBG 9220253.1)	AU: QLD; Cook; Mount Elliot
<i>Dipodium</i> <i>ammolithum</i>	HTCG 1372	M.D. Barrett 4910A (PERTH)	AU: WA; North Kimberley, Theda Station
<i>Dipodium</i> <i>atropurpureum</i> 1	HTCG 0760	W.M. Dowling DC 1717 (CANB 924629.1)	AU: NSW; Northern Tablelands; Barrington Tops State Forest
<i>Dipodium</i> <i>atropurpureum</i> 2	HTCG 1679	M.A. Clements 4426 (CBG 8605570.1)	AU: NSW; Northern Tablelands; New England Highway to Armidale
<i>Dipodium</i> <i>basalticum</i>	HTCG 1693	D.E. Murfet 4837 (CANB 662327.1)	AU: NT; Darwin and Gulf; near Nhulunbuy
<i>Dipodium</i> <i>campanulatum</i> 1	HTCG 1680	K. Alcock DLJ5622 (CBG 9004646.2)	AU: SA; South-east; Naracoorte
<i>Dipodium</i> <i>campanulatum</i> 2	HTCG 1681	D.E. Murfet 1930b (CANB 677107.2)	AU: SA; South-east; Penola Conservation Park
<i>Dipodium</i> <i>elegantulum</i>	HTCG 1682	L. Lawler 8 (CBG 8605836.1)	AU: QLD; Cook; near Mareeba
<i>Dipodium</i> <i>ensifolium</i>	HTCG 1343	D.M. Crayn 1581 (CNS 145658.1)	AU: QLD; Cook; record is Queensland sensitive
<i>Dipodium</i> <i>hamiltonianum</i>	HTCG 1683	D.L. Jones & P.D. Jones s.n. (CANB)	AU: QLD; Moreton; Currimundi
<i>Dipodium</i> <i>interaneum</i>	HTCG 0181	J. Egan ORG7745 (CANB)	AU: ACT; Canberra; Birrigai
<i>Dipodium</i> <i>pandanum</i> 1	CNS_G01262	B. Gray 8233 (CANB 572368.2)	AU: QLD; Kennedy North; near Coen; record is Queensland sensitive

<i>Dipodium pandanum</i> 2	HTCG 1694	M. Jacobs 8984 (CANB 576763.1)	PG: Mount Bosavi
<i>Dipodium pardalinum</i> 1	HTCG 1684	D.L. Jones 12834 (CBG 9603749.1)	AU: Vic; Victorian Volcanic Plain; Heathmere
<i>Dipodium pardalinum</i> 2	HTCG 1685	D.L. Jones 12830 (CBG 9603745.1)	AU: Vic; Victorian Volcanic Plain; Heathmere
<i>Dipodium pulchellum</i>	HTCG 1686	D.L. Jones s.n. (CANB)	AU: QLD; Moreton; Green Mountains
<i>Dipodium punctatum</i>	HTCG 0827	C. Bower ORG7816 (CANB 906469.1)	AU: NSW; Central Tablelands; Black Salee Reserve
<i>Dipodium roseum</i> 1	HTCG 1687	C. Houston ORG3859 (CANB 656733.1)	AU: SA; Lofty South; Wotton Scrub
<i>Dipodium roseum</i> 2	HTCG 1688	C. Houston ORG3859 (CANB 656733.2)	AU: SA; Lofty South; Wotton Scrub
<i>Dipodium stenocheilum</i> 1	HTCG 1689	M.A. Clements 1189 (CBG 7801007.1)	AU: NT; Darwin and Gulf; Elcho Island
<i>Dipodium stenocheilum</i> 2	HTCG 1690	D.E. Murfet 3018 (CANB 619696.1)	AU: NT; Darwin and Gulf; Livingston
<i>Dipodium variegatum</i>	HTCG 1692	D.L. Jones 1280 (CANB 665182.1)	AU: QLD; Moreton; Beenleigh

Outgroup

<i>Acriopsis emarginata</i>	CNS_G00305	C.D. Kilgour 634A (CNS 135324.1)	AU: QLD, Cook, Daintree National Park
<i>Cymbidium canaliculatum</i>	CNS_G00165	K.R. McDonald, 11722 (BRI AQ0831415)	AU: QLD, Cook, Mungkan Kandju National Park
<i>Eulophia bicallosa</i>	HTCG 1696	I. Morris (DLJ 4579) (CBG 8913381.1)	AU: NT; Darwin and Gulf; Howard Springs
<i>Eulophia graminea</i>	CNS_G02766	C.P. Brock 311 (CANB 596921.1)	AU: NT; Darwin
<i>Eulophia nuda</i>	HTCG 1697	R. Crane 1072 (CANB)	cult. ex AU: QLD; Moreton; Caloundra
<i>Geodorum densiflorum</i>	CNS_G01890	K. Schulte 254B (CNS 146066.1)	AU: QLD; Cairns region
<i>Oeceoclades pelorica</i>	HTCG 1695	J. Taylor s.n. (CBG 7905124.1)	cult. ex AU: QLD; Cook; Iron Range

Table 2. Comparison of plastome features in *Dipodium*.

Sample	Plastome Length (bp)	SSC length (bp)	IRA/B length (bp)	LSC length (bp)	GC content	Total CDS (unique CDS)	Total tRNA (unique tRNA)	Total rRNA (unique rRNA)	Total pseudo-genes	Total lost genes	Total functional genes
<i>D. pandanum</i> 1	146,204	13,849	24,762	82,831	37.0%	74 (68)	38 (30)	8 (4)	9	3	120
<i>D. ensifolium</i>	150,084	16,756	25,497	82,334	36.9%	74 (68)	38 (30)	8 (4)	10	3	120
<i>D. hamiltonianum</i> complex											
<i>D. hamiltonianum</i>	145,902	14,384	24,929	81,660	37.1%	74 (68)	39 (31)	8 (4)	10	3	121
<i>D. interaneum</i>	146,497	14,635	24,951	81,960	37.0%	74 (68)	39 (31)	8 (4)	10	3	121
<i>D. stenocheilum</i> complex											
<i>D. elegantulum</i>	144,865	14,003	24,606	81,650	36.9%	74 (68)	39 (31)	8 (4)	9	4	121
<i>D. stenocheilum</i> 2	145,589	13,821	25,127	81,514	37.0%	74 (68)	39 (31)	8 (4)	9	4	121
<i>D. stenocheilum</i> 1	144,751	12,670	25,009	82,063	36.9%	74 (68)	38 (30)	8 (4)	9	4	120
<i>D. basalticum</i>	148,478	15,238	25,640	81,960	37.0%	74 (68)	38 (30)	8 (4)	10	3	120
<i>D. ammolithum</i>	147,842	14,697	25,600	81,946	37.0%	74 (68)	39 (31)	8 (4)	9	4	121
<i>D. variegatum</i>	142,949	12,039	24,436	82,038	37.0%	74 (68)	38 (30)	8 (4)	6	7	120
<i>D. punctatum</i> complex											
<i>D. pulchellum</i>	151,425	15,735	26,369	82,952	36.9%	74 (68)	38 (30)	8 (4)	11	2	120
<i>D. punctatum</i>	151,181	15,737	26,136	83,172	37.0%	74 (68)	38 (30)	8 (4)	11	2	120
<i>D. campanulatum</i> 1	146,390	13,602	25,284	82,220	36.9%	74 (68)	37 (29)	8 (4)	12	2	119
<i>D. campanulatum</i> 2	149,050	14,266	25,902	82,980	37.0%	74 (68)	38 (30)	8 (4)	11	2	120
<i>D. roseum</i> complex											
<i>D. atropurpureum</i> 2	149,390	15,509	25,909	82,063	36.9%	74 (68)	38 (30)	8 (4)	10	3	120
<i>D. atropurpureum</i> 1	150,481	15,633	26,399	82,050	36.9%	74 (68)	38 (30)	8 (4)	9	4	120
<i>D. aff. roseum</i> 4	152,282	16,426	26,630	82,596	36.9%	73 (67)	38 (30)	8 (4)	11	3	119
<i>D. aff. roseum</i> 2	150,462	15,514	26,388	82,172	36.9%	74 (68)	38 (30)	8 (4)	9	4	120
<i>D. aff. roseum</i> 3	152,956	16,571	26,817	82,751	36.9%	74 (68)	38 (30)	8 (4)	10	3	120
<i>D. aff. roseum</i> 1	151,791	16,362	26,424	82,581	36.9%	74 (68)	38 (30)	8 (4)	10	3	120
<i>D. pardalinum</i> 2	151,659	16,276	26,580	82,223	36.9%	74 (68)	38 (30)	8 (4)	10	3	120
<i>D. pardalinum</i> 1	148,174	15,283	25,494	81,903	36.8%	74 (68)	38 (30)	8 (4)	9	4	120
<i>D. roseum</i> 1	150,857	15,848	26,521	81,967	36.9%	74 (68)	38 (30)	8 (4)	9	4	120
<i>D. roseum</i> 2	147,730	14,192	25,819	81,900	36.8%	74 (68)	38 (30)	8 (4)	9	4	120

1 **Table 3.** List of genes identified in the plastomes of *Dipodium*.

Gene group	Gene name
Transfer RNA genes	<i>trnA</i> -UGC ^{*a} , <i>trnC</i> -GCA, <i>trnD</i> -GUC ^d , <i>trnE</i> -UUC, <i>trnF</i> -GAA, <i>trnI</i> M-CAU, <i>trnG</i> -GCC, <i>trnG</i> -UCC [*] , <i>trnH</i> -GUG ^a , <i>trnI</i> -CAU ^a , <i>trnI</i> -GAU ^{*a} , <i>trnK</i> -UUU [*] , <i>trnL</i> -CAA ^a , <i>trnL</i> -UAA [*] , <i>trnL</i> -UAG, <i>trnM</i> -CAU, <i>trnN</i> -GUU ^a , <i>trnP</i> -UGG, <i>trnQ</i> -UUG, <i>trnR</i> -ACG ^a , <i>trnR</i> -UCU, <i>trnS</i> -GCU, <i>trnS</i> -GGA, <i>trnS</i> -UGA, <i>trnT</i> -GGU, <i>trnT</i> -UGU, <i>trnV</i> -GAC ^{ab} , <i>trnV</i> -UAC [*] , <i>trnW</i> -CCA, <i>trnY</i> -GUA
Small subunit of ribosome	<i>rps2</i> , <i>rps3</i> , <i>rps4</i> , <i>rps7</i> ^a , <i>rps8</i> , <i>rps11</i> , <i>rps12</i> ^{*a} , <i>rps14</i> , <i>rps15</i> , <i>rps16</i> [*] , <i>rps18</i> , <i>rps19</i> ^a
Large subunit of ribosome	<i>rpl2</i> ^{*a} , <i>rpl14</i> , <i>rpl16</i> [*] , <i>rpl20</i> , <i>rpl22</i> , <i>rpl23</i> ^a , <i>rpl32</i> , <i>rpl33</i> , <i>rpl36</i>
DNA-dependent RNA polymerase	<i>rpoA</i> , <i>rpoB</i> , <i>rpoC1</i> [*] , <i>rpoC2</i>
Genes for photosynthesis	
Subunits of photosynthesis I	<i>psaA</i> , <i>psaB</i> , <i>psaC</i> , <i>psaI</i> , <i>psaJ</i>
Subunits of photosynthesis II	<i>psbA</i> , <i>psbB</i> , <i>psbC</i> , <i>psbD</i> , <i>psbE</i> , <i>psbF</i> , <i>psbH</i> , <i>psbI</i> , <i>psbJ</i> , <i>psbK</i> , <i>psbL</i> , <i>psbM</i> , <i>psbN</i> , <i>psbT</i> , <i>psbZ</i>
Subunit of Cytochrome b6f	<i>petA</i> , <i>petB</i> [*] , <i>petD</i> [*] , <i>petG</i> , <i>petL</i> , <i>petN</i>
Subunit of ATP synthase	<i>atpA</i> , <i>atpB</i> , <i>atpE</i> , <i>atpF</i> [*] , <i>atpH</i> , <i>atpI</i>
Subunit of NADH dehydrogenase	<i>ndhA</i> ^{*c} , <i>ndhB</i> ^{*ac} , <i>ndhC</i> ^c , <i>ndhD</i> ^c , <i>ndhE</i> ^c , <i>ndhF</i> ^c , <i>ndhG</i> ^c , <i>ndhH</i> ^c , <i>ndhI</i> ^c , <i>ndhJ</i> ^c , <i>ndhK</i> ^c
Large subunits of RubisCO	<i>rbcL</i>
Ribosomal RNA genes	<i>rrn5</i> ^a , <i>rrn4.5</i> ^a , <i>rrn16</i> ^a , <i>rrn23</i> ^a
Other genes	
Maturase	<i>matK</i>
Envelope membrane protein	<i>cemA</i> ^c
Subunit of acetyl-CoA carboxylase	<i>accD</i>
C-type cytochrome synthesis gene	<i>cssA</i>
Protease	<i>clpP</i> [*]
Translation initiation factor IF-1	<i>infA</i>
<i>ycf</i> genes	<i>ycf1</i> , <i>ycf2</i> ^a , <i>ycf3</i> [*] , <i>ycf4</i>

2 ^aDuplicated gene. ^bTriplicated gene in *D. hamiltonianum*, *D. interaneum*, *D. elegantulum*, *D.*
3 *stenocheilum* 2, *D. ammolithum*. ^cPseudogene or lost. ^dPseudogene in *D. campanulatum* 1. ^ePseudogene
4 in *D. aff. roseum* 4. *Intron-containing gene.

5
6
7
8
9
10
11
12
13
14

15 **Funding**

16 This study was supported by the Australian Biological Resources Study (Dept. of Agriculture,
17 Water and the Environment, Australian Government NTRGP BBR210-34) and the Australian
18 Orchid Foundation (AOF325.18; AOF357.23). SG received research grant from the Australian
19 Tropical Herbarium.

20 **Conflict of Interest**

21 The authors declare that the research was conducted in the absence of any commercial or
22 financial relationships that could be construed as a potential conflict of interest.

23 **Author Contributions**

24 **Conceptualisation:** SG, KN, MAC. **Methodology:** SG, KN, SJB; **Data curation:** SG, KN,
25 MAC. **Formal analysis:** SG, SJB. **Funding acquisition:** KN, DMC, MAC, SG.
26 **Investigation:** SG, KN, MAC, SJB, JAN, VSP, PMS. **Visualisation:** SG. **Writing – original**
27 **draft:** SG. **Writing – review & editing:** SG, KN, MAC, SJB, JAN, VSP, PMS, DMC.

28

29 **Acknowledgements**

30 The authors acknowledge the contribution of Bioplatforms Australia (enabled by NCRIS) in
31 the generation of data used in this publication. We acknowledge K. Alcock, M.D. Barrett, C.
32 Bower, C.P. Brock, R. Crane, D.M. Crayn, W. Dowling, J. Egan, B. Gray, C. Houston, M.
33 Jacobs, D.L. Jones, P.D. Jones, C.D. Kilgour, L. Lawler, K.R. McDonald, I. Morris, D.E.
34 Murfet, J. Taylor for collection of plant material used in this study.

35 **Supplementary Material**

36 **Supplementary Material 1.** Details of samples included in phylogenetic analysis and
37 divergence-time estimations.

38

39 **Supplementary Material 2. a.** Details of plastid loci included in alignment of ML-
40 phylogenetic and divergence-time estimations. **b.** Parsimony informative sites (Pi) for each
41 plastid gene.

42

43 **Supplementary Material 3.** ML-Phylogenetic tree of Orchidaceae.

44

45 **Supplementary Material 4. a.** Model comparison by AICM (Akaike Information Criterion by
46 MCMC) **b.** Comparison divergence-time estimations of major Orchidaceae lineages
47 (subfamilies), the tribe Cymbidieae and subtribe Dipodiinae.

48

49 **Supplementary Material 5.** Maximum-clade-credibility tree from Bayesian divergence-time
50 estimations of Orchidaceae.

51

52 **Supplementary Material 6.** Summary of assembly features of 24 newly generated *Dipodium*
53 plastomes.

54

55 **Supplementary Material 7.** Circular plastome maps of 24 newly generated *Dipodium*
56 plastomes.

57

58 **References**

59 ALA (2023). Atlas of Living Australia. Available at: <https://www.ala.org.au> (Accessed August,8
60 2023).

61

62 APC (2023): Australian Plant Census. Available at: biodiversity.org.au/nsl/services/search/taxonomy
63 (Accessed May 5, 2023).

64

65 Altschul, S.F., Gish, W., Miller, W., Myers, E.W., Lipman, D.J. (1990). Basic local alignment search
66 tool. *J. Mol. Biol.* 215, 403–410. doi.org/10.1016/S0022-2836(05)80360-2

67

68 Bankevich, A., Nurk, S., Antipov, D., Gurevich, A.A., Dvorkin, M., Kulikov, A.S., Lesin, V.M.,
69 Nikolenko, S.I., Pham, S., Prjibelski, A.D., Pyshkin, A.V., Sirotkin, A.V., Vyahhi, N., Tesler, G.,
70 Alekseyev, M.A., Pevzner, P.A. (2012). SPAdes: A new genome assembly algorithm and its
71 applications to single-cell sequencing. *J. Comput. Biol.* 19, 455–477. doi.org/10.1089/cmb.2012.0021

72

73 Barrett, C.F., Freudenstein, J.V., Li, J., Mayfield-Jones, D.R., Perez, L., Pires, J.C., Santos, C. (2014).
74 Investigating the path of plastid genome degradation in an early-transitional clade of heterotrophic
75 orchids, and implications for heterotrophic angiosperms. *Mol. Biol. Evol.* 31, 3095–3112.
76 doi.org/10.1093/molbev/msu252

77

78 Barrett, C.F., Wicke, S., Sass, C. (2018). Dense infraspecific sampling reveals rapid and independent
79 trajectories of plastome degradation in a heterotrophic orchid complex. *New Phytol.* 218, 1192–1204.
80 doi.org/10.1111/nph.15072

81

82 Barrett, C.F., Sinn, B.T., Kennedy, A.H. (2019). Unprecedented parallel photosynthetic losses in a
83 heterotrophic orchid genus. *Mol. Biol. Evol.* 36, 1884–1901. doi.org/10.1093/molbev/msz111

84

85 Barrett, R. L., Barrett, M.D., Clements, M.A. (2022). A revision of Orchidaceae from the Kimberley
86 region of Western Australia with new species of tropical *Calochilus* and *Dipodium*. *Telopea* 25, 203–
87 270. doi.org/10.7751/telepea15711

88

89 Batista, J.A.N., Mota, A.C.M., Proite, K., Bianchetti, L.D.B., Romero-González, G.A., Huerta, H.,
90 Salazar, G.A. (2014). Molecular phylogenetics of neotropical *Cyanaeorchis* (Cymbidieae,
91 Epidendroideae, Orchidaceae): geographical rather than morphological similarities plus a new species.
92 *Phytotaxa* 156, 251–272. doi.org/10.11646/phytotaxa.156.5.1

93

94 Bolger, A.M., Lohse, M., Usadel, B. (2014). Trimmomatic: a flexible trimmer for Illumina sequence
95 data. *Bioinformatics* 30, 2114–2120. doi.org/10.1093/bioinformatics/btu170

96

97 Bouckaert, R., Heled, J., Suchard, M.A., Rambaut, A., Drummond, A.J. (2014). BEAST 2: A software
98 platform for Bayesian evolutionary analysis. *PLOS Comput. Biol.* 10, 4.

99 doi.org/10.1371/journal.pcbi.1003537

- 100
101 Bouckaert, R., Vaughan, T.G., Barido-Sottani, J., Duchêne, S., Fourment, M., Gavryushkina, A., Heled,
102 J., Jones, G., Kühnert, D., De Maio, N., Matschiner, M., Mendes, F.K., Müller, N.F., Ogilvie, H.A., du
103 Plessis, L., Poppinga, A., Rambaut, A., Rasmussen, D., Siveroni, I., Suchard, M.A., Wu, C.H., Xie, D.,
104 Zhang, C., Stadler, T., Drummond, A.J. (2019). BEAST 2.5: An advanced software platform for
105 Bayesian evolutionary analysis. *PLoS Comput. Biol.* 15, 4. doi.org/10.1371/journal.pcbi.1006650
106
107 Bougoure, J.J., Dearnaley, J.D.W (2005). The fungal endophytes of *Dipodium variegatum*
108 (Orchidaceae). *Australasian Mycologist* 24, 15–19.
109
110 Bushnell, B. (2014). BBMap: A fast, accurate, splice-aware aligner. Lawrence Berkeley National
111 Laboratory, Berkeley, CA (United States).
112
113 Braukmann, T.W.A., Broe, M.B., Stefanović, S. and Freudenstein, J.V. (2017). On the brink: the highly
114 reduced plastomes of nonphotosynthetic Ericaceae. *New Phytol.* 216, 254-266.
115 doi.org/10.1111/nph.14681
116
117 Byrne, M., Yeates, D.K., Joseph, L., Kearney, M., Bowler, J., Williams, M.A.J., Cooper, S., Donnellan,
118 S.C., Keogh, J.S., Leys, R., Melville, J., Murphy, D.J., Porch, N. and Wyrwoll, K.-H. (2008). Birth of
119 a biome: insights into the assembly and maintenance of the Australian arid zone biota. *Mol. Ecol.* 17,
120 4398–4417. doi.org/10.1111/j.1365-294X.2008.03899.x
121
122 Chase, M.W., Cameron, K.M., Freudenstein, J.V., Pridgeon, A.M., Salazar, G., Van den Berg C.,
123 Schuiteman, A. (2015). An updated classification of Orchidaceae. *Bot. J. Linn. Soc.* 177, 151–174.
124 doi.org/10.1111/boj.12234
125
126 Christenhusz, M.J.M, Byng, J.W. (2016). The number of known plants species in the world and its
127 annual increase. *Phytotaxa* 261, 201. doi.org/10.11646/phytotaxa.261.3.1.
128
129 Crayn, D.M., Costion, C., Harrington, M.G. (2015). The Sahul–Sunda floristic exchange: dated
130 molecular phylogenies document Cenozoic intercontinental dispersal dynamics. *J. Biogeog.* 42, 11–24.
131 dx.doi.org/10.1111/jbi.12405
132
133 Dearnaley, J.D.W., Le Brocq, A.F. (2006). Molecular identification of the primary root fungal
134 endophytes of *Dipodium hamiltonianum* (Orchidaceae). *Aust. J. Bot.* 54, 487.
135 doi.org/10.1071/BT05149
136
137 Delannoy, E., Fujii, S., Colas des Francs-Small, C., Brundrett, M., Small, I. (2011). Rampant gene loss
138 in the underground orchid *Rhizanthella gardneri* highlights evolutionary constraints on plastid
139 genomes. *Mol. Biol. Evol.* 28, 2077–2086. doi.org/10.1093/molbev/msr028
140
141 Douglas, J., Zhang, R., Bouckaert, R. (2021). Adaptive dating and fast proposals: Revisiting the
142 phylogenetic relaxed clock model. *PLoS Comput. Biol.* 17 (2). doi.org/10.1371/journal.pcbi.1008322
143
144 Dong, W.L., Wang, R.N., Zhang, N.Y., Fan, W.B., Fang, M.F., Li, Z.H. (2018). Molecular evolution
145 of chloroplast genomes of orchid species: insights into phylogenetic relationship and adaptive
146 evolution. *Int. J. Mol. Sci.* 19, 716. doi.org/10.3390/ijms19030716
147
148 Drummond, A.J., Rambaut, A. (2007). BEAST: Bayesian evolutionary analysis by sampling trees.
149 *BMC Evol. Biol.* 7, 214. doi.org/10.1186/1471-2148-7-214
150
151 Fabozzi, F.J., Focardi, S.M., Rachev, S.T., Arshanapalli, B.G. (2014). Appendix E. Model Selection
152 Criterion: AIC and BIC in “The basics of financial econometrics: tools, concepts, and asset management
153 applications.” John Wiley & Sons, Inc. 399–403.
154

- 155 Feng, Y.L., Wicke, S., Li, J.W., Han, Y., Lin, C.S., Li, D.Z., Zhou, T.T., Huang, W.C., Huang, L.Q.,
156 Jin, X.H. (2016). Lineage-specific reductions of plastid genomes in an orchid tribe with partially and
157 fully mycoheterotrophic species. *Genome Biol. Evol.* 8, 2164–2175. doi.org/10.1093/gbe/evw144
158
- 159 Freudenstein, J.V., Chase, M.W. (2015). Phylogenetic relationships in Epidendroideae (Orchidaceae),
160 one of the great flowering plant radiations: progressive specialization and diversification. *Ann. Bot.* 115,
161 665–681. doi.org/10.1093/aob/mcu253
162
- 163 Gallagher, S.J., Greenwood, D.R., Taylor, D., Smith, A.J., Wallace, M.W., Holdgate, G.R. (2003). The
164 Pliocene climatic and environmental evolution of southeastern Australia: Evidence from the marine and
165 terrestrial realm. *Palaeogeogr., Palaeoclimatol., Palaeoecol.* 193, 349–382.
166 doi.org/10.1016/S0031-0182(03)00231-1
167
- 168 Gernhard, T. (2008). The conditioned reconstructed process. *J. Theor. Biol.* 253, 769–778.
169 doi.org/10.1016/j.jtbi.2008.04.005
170
- 171 Givnish, T.J., Zuluaga, A., Spalink, D., Soto Gomez, M., Lam, V.K.Y., Saarela, J.M., Sass, C., Iles,
172 W.J.D., De Sousa, D.J.L., Leebens-Mack, J., Chris Pires, J., Zomlefer, W.B., Gandolfo, M.A., Davis,
173 J.I., Stevenson, D.W., De Pamphilis, C., Specht, C.D., Graham, S.W., Barrett, C.F., Ané, C. (2018).
174 Monocot plastid phylogenomics, timeline, net rates of species diversification, the power of multi-gene
175 analyses, and a functional model for the origin of monocots. *Am. J. Bot.* 105, 1888–1910.
176 doi.org/10.1002/ajb2.1178
177
- 178 Givnish, T.J., Spalink, D., Ames, M., Lyon, S.P., Hunter, S.J., Zuluaga, A., Iles, W.J.D., Clements,
179 M.A., Arroyo, M.T.K., Leebens-Mack, J., Endara, L., Kriebel, R., Neubig, K.M., Whitten, W.M.,
180 Williams, N.H., Cameron, K.M. (2015). Orchid phylogenomics and multiple drivers of their
181 extraordinary diversification. *Proc. Royal Soc. B* 282, 20151553. doi.org/10.1098/rspb.2015.1553
182
- 183 Górnaiak, M., Paun, O., Chase, M.W. (2010). Phylogenetic relationships within Orchidaceae based on a
184 low-copy nuclear coding gene, *Xdh*: Congruence with organellar and nuclear ribosomal DNA results.
185 *Mol. Phy. Evol.* 56, 784–795. doi.org/10.1016/j.ympcv.2010.03.003
186
- 187 Graham, S.W., Lam, V.K.Y., Merckx, V.S.F.T (2017). Plastomes on the edge: the evolutionary
188 breakdown of mycoheterotroph plastid genomes. *New Phytol.* 214, 48–55. doi.org/10.1111/nph.14398
189
- 190 Greiner, S., Lehwark, P., Bock, R. (2019). OrganellarGenomeDRAW (OGDRAW) version 1.3.1:
191 expanded toolkit for the graphical visualization of organellar genomes. *Nucleic Acids Res.* 47, W59–
192 W64. doi.org/10.1093/nar/gkz238
193
- 194 Guindon, S., Dufayard, J.-F., Lefort, V., Anisimova, M., Hordijk, W., Gascuel, O. (2010). New
195 algorithms and methods to estimate maximum-likelihood phylogenies: Assessing the performance of
196 PhyML 3.0. *Syst. Biol.* 59, 307–321. doi.org/10.1093/sysbio/syq010
197
- 198 He, Y., Wang, H. (2021). Terrestrial material input to the northwest shelf of Australia through the
199 Pliocene-Pleistocene period and its implications on continental climates. *Geophys. Res. Lett.*, 48,
200 e2021GL092745. doi.org/10.1029/2021GL092745
201
- 202 Hoang, D.T., Chernomor, O., Von Haeseler, A., Minh, B.Q., Vinh, L.S. (2018). UFBoot2: Improving
203 the Ultrafast Bootstrap approximation. *Mol. Biol. Evol.* 35, 518–522. doi.org/10.1093/molbev/msx281
204
- 205 Jacquemyn, H., Merckx, V.S.F.T (2019). Mycorrhizal symbioses and the evolution of trophic modes in
206 plants (R Shefferson, Ed.). *J. Ecol.* 107, 1567–1581. doi.org/10.1111/1365-2745.13165
207
- 208 Jones, D.L. (2021). A complete guide to native orchids of Australia. Sydney: Reed New Holland
209 Publishers.

- 210
211 Jones, D.L. and Clements, M.A. (1987). New orchid taxa from south-eastern Queensland. *Proc. R. Soc.*
212 *Queensland* 98, 128.
213
214 Joyce, E.M., Crayn, D.M., Lam, V.K.Y., Gerelle, W.K., Graham, S.W., Nauheimer, L. (2018). Evolution
215 of *Geosiris* (Iridaceae): historical biogeography and plastid-genome evolution in a genus of non-
216 photosynthetic tropical rainforest herbs disjunct across the Indian Ocean. *Aust. Syst. Bot.* 31, 504–522.
217 doi.org/10.1071/SB18028
218
219 Joyce, E.M., Thiele, K.R., Slik, J.W.F., Crayn, D.M. (2021a). Plants will cross the lines: climate and
220 available land mass are the major determinants of phytogeographical patterns in the Sunda–Sahul
221 Convergence Zone. *Biol. J. Linn. Soc.* 132, 374–387. doi.org/10.1093/biolinnean/blaa194
222
223 Joyce, E.M., Pannell, C.M., Rossetto, M., Yap, J.Y.S., Thiele, K.R., Wilson, P.D., Crayn, D.M. (2021b).
224 Molecular phylogeography reveals two geographically and temporally separated floristic exchange
225 tracks between Southeast Asia and Northern Australia. *J. Biogeog.* 48, 1213–1227.
226 doi.org/10.1111/jbi.14072
227
228 Kalyanamoorthy, S., Minh, B.Q., Wong, T.K.F., Von Haeseler, A., Jermini, L.S. (2017). ModelFinder:
229 fast model selection for accurate phylogenetic estimates. *Nat. Methods* 14, 587–589.
230 doi.org/10.1038/nmeth.4285
231
232 Katoh, K., Misawa, K., Kuma, K., Miyata, T., MAFFT (2002). A novel method for rapid multiple
233 sequence alignment based on fast Fourier transform, *Nucleic Acids Res.* 30 (14), 3059–3066,
234 doi.org/10.1093/nar/gkf436
235
236 Katoh, K., Standley, D.M. (2013). MAFFT Multiple Sequence Alignment Software Version 7:
237 Improvements in performance and usability. *Mol. Biol. Evol.* 30, 772–780.
238 <https://doi.org/10.1093/molbev/mst010>
239
240 Kim, H.T., Kim, J.S., Moore, M.J., Neubig, K.M., Williams, N.H., Whitten, W.M., Kim, J.H. (2015).
241 Seven new complete plastome sequences reveal rampant independent loss of the *ndh* gene family across
242 orchids and associated instability of the inverted repeat/small single-copy region Boundaries (S. Aceto,
243 Ed.). *PLOS ONE* 10, e0142215. doi.org/10.1371/journal.pone.0142215
244
245 Kim, H.T., Chase, M.W. (2017). Independent degradation in genes of the plastid *ndh* gene family in
246 species of the orchid genus *Cymbidium* (Orchidaceae; Epidendroideae). *PLOS ONE* 12, e0187318.
247 doi.org/10.1371/journal.pone.0187318
248
249 Kim, Y.K., Kwak, M.H., Chung, M.G., Kim, H.W., Jo, S., Sohn, J.Y., Cheon, S.H., Kim, K.J. (2017)
250 The complete plastome sequence of the endangered orchid *Cymbidium macrorhizon* (Orchidaceae).
251 *Mitochondrial DNA Part B* 2, 725–727. doi.org/10.1080/23802359.2017.1390411
252
253 Kim, Y.K., Jo, S., Cheon, S.H., Joo, M.J., Hong, J.R., Kwak, M.H., Kim, K.J. (2019). Extensive losses
254 of photosynthesis genes in the plastome of a mycoheterotrophic orchid, *Cyrtosia septentrionalis*
255 (Vanilloideae: Orchidaceae). *Genome Biol. Evol.* 11(2), 565–571. <https://doi.org/10.1093/gbe/evz024>
256
257 Kim, Y.K., Jo, S., Cheon, S.H., Joo, M.J., Hong, J.R., Kwak, M., Kim, K.J. (2020). Plastome evolution
258 and phylogeny of Orchidaceae, with 24 new sequences. *Front. Plant Sci.* 11, 22.
259 <https://doi.org/10.3389/fpls.2020.00022>
260
261 Kim, Y.K., Cheon, S.-H., Hong, J.-R., Kim, K.J. (2023). Evolutionary Patterns of the Chloroplast
262 Genome in Vanilloid Orchids (Vanilloideae, Orchidaceae). *Int. J. Mol. Sci.* 24, 3808.
263 doi.org/10.3390/ijms24043808
264

- 265 Klimpert, N.J., Mayer, J.L.S., Sarzi, D.S., Prosdocimi, F., Pinheiro, F., Graham, S.W. (2022).
266 Phylogenomics and plastome evolution of a Brazilian mycoheterotrophic orchid, *Pogoniopsis*
267 *schenckii*. *Am. J. Bot.* 109(12), 2030–2050. doi.org/10.1002/ajb2.16084
268
- 269 Könyves, K., Bilsborrow, J., Christodoulou, M.D., Culham, A., David, J. (2021). Comparative
270 plastomics of Amaryllidaceae: inverted repeat expansion and the degradation of the *ndh* genes in
271 *Strumaria truncate* Jacq. *PeerJ* 9, e12400. doi.org/10.7717/peerj.12400
272
- 273 Lam, V.K.Y., Gomez, M.S., Graham, S.W. (2015). The highly reduced plastome of mycoheterotrophic
274 *Sciaphila* (Triuridaceae) is colinear with its green relatives and is under strong purifying selection,
275 *Genome Biol. Evol.* 7, 2220–2236. <https://doi.org/10.1093/gbe/evv134>
276
- 277 Lallemand, F., Logacheva, M., Le Clainche, I., Bérard, A., Zheleznaia, E., May, M., Jakalski, M.,
278 Delannoy, É., Le Paslier, M.C., Selosse, M.A. (2019). Thirteen new plastid genomes from mixotrophic
279 and autotrophic species provide insights into heterotrophy evolution in Neottieae orchids. *Genome Biol.*
280 *Evol.* 11, 2457–2467. doi.org/10.1093/gbe/evz170
281
- 282 Li, M.H., Zhang, G.Q., Liu, Z.J., Lan, S.R. (2016). Subtribal relationships in Cymbidieae
283 (Epidendroideae, Orchidaceae) reveal a new subtribe, Dipodiinae, based on plastid and nuclear coding
284 DNA. *Phytotaxa* 246, 37. doi.org/10.11646/phytotaxa.246.1.3
285
- 286 Li, X., Yang, J.B., Wang, H., Song, Y., Corlett, R.T., Yao, X., Li, D.Z., Yu, W.B. (2021). Plastid NDH
287 pseudogenization and gene loss in a recently derived lineage from the largest hemiparasitic plant genus
288 *Pedicularis* (Orobanchaceae). *Plant Cell Physiol.* 62, 971–984. doi.org/10.1093/pcp/pcab074
289
- 290 Li, Z.H., Jiang, Y., Ma, X., Li, J.W., Yang, J.B., Wu, J.Y., Jin, X.H. (2020). Plastid genome evolution
291 in the subtribe Calypsoinae (Epidendroideae, Orchidaceae) (J Archibald, Ed.). *Genome Biol. Evol.* 12,
292 867–870. doi.org/10.1093/gbe/evaa091
293
- 294 Lin, C.S., Chen, J.J., Huang, Y.T., Chan, M.T., Daniell, H., Chang, W.J., Hsu, C.T., Liao, D.C., Wu,
295 F.H., Lin, S.Y., Liao, C.F., Deyholos, M.K., Wong, G.K., Albert, V.A., Chou, M.L., Chen, C.Y., Shih,
296 M.C. (2015). The location and translocation of *ndh* genes of chloroplast origin in the Orchidaceae
297 family. *Sci. Rep.* 12; 5:9040. doi.org/10.1038/srep09040
298
- 299 Logacheva, M.D., Schelkunov, M.I., Aleksey, A. P. (2011). Sequencing and analysis of plastid genome
300 in mycoheterotrophic orchid *Neottia nidus-avis*. *Genome Biol. Evol.* 3, 1296–1303.
301 doi.org/10.1093/gbe/evr102
302
- 303 Martin, H.A. (2006). Cenozoic climatic change and the development of the arid vegetation in Australia.
304 *J. Arid Environ.* 66, 533–563. doi.org/10.1016/j.jaridenv.2006.01.009
305
- 306 McLay, T.G. B., Bayly, M. J., Whitehead, M. R., Fowler, R. M. (2023). Retention of an apparently
307 functional plastome in an apparently mycoheterotrophic orchid, *Dipodium roseum* D.L.Jones &
308 M.A.Clem. (Orchidaceae). *Aust. J. Bot.* 71, 306–317. doi.org/10.1071/BT22075
309
- 310 Merckx, V.S.F.T. (2013). *Mycoheterotrophy: an introduction in Mycoheterotrophy. The Biology of*
311 *Plants Living on Fungi*. Berlin: Springer-Verlag 297–342.
312 doi.org/10.1007/978-1-4614-5209-6
313
- 314 Minh, B.Q., Schmidt, H.A., Chernomor, O., Schrempf, D., Woodhams, M.D., Von Haeseler, A.,
315 Lanfear, R. (2020). IQ-TREE 2: New Models and efficient methods for phylogenetic inference in the
316 genomic era. *Mol. Biol. Evol.* 37, 1530–1534. doi.org/10.1093/molbev/msaa015
317

- 318 Nargar, K., O'Hara, K., Mertin, A., Bent, S.J., Nauheimer, L., Simpson, L., Zimmer, H., Molloy, B.P.J.,
319 Clements, M.A. (2022). Evolutionary relationships and range evolution of greenhood orchids (subtribe
320 Pterostylidinae): Insights from plastid phylogenomics. *Front. Plant Sci.* 13:912089.
321 doi.org/10.3389/fpls.2022.912089
322
- 323 NCBI (2022), National Library of Medicine. Available at: <https://www.ncbi.nlm.nih.gov> (Accessed
324 June 2, 2022)
325
- 326 Nguyen, L.T., Schmidt, H.A., Von Haeseler, A., Minh, B.Q. (2015). IQ-TREE: A fast and effective
327 stochastic algorithm for estimating maximum-likelihood phylogenies. *Mol. Biol. Evol.* 32, 268–274.
328 doi.org/10.1093/molbev/msu300
329
- 330 Niu, Z., Xue, Q., Zhu, S., Sun, J., Liu, W., Ding, X. (2017). The complete plastome sequences of four
331 orchid species: Insights into the evolution of the Orchidaceae and the utility of plastomic mutational
332 hotspots. *Front. Plant Sci.* 8, 715. doi.org/10.3389/fpls.2017.00715
333
- 334 O'Byrne, P. (2014). On the evolution of *Dipodium* R. Br. *Reinwardtia* 14 (1), 123–132 [https://e-](https://e-journal.biologi.lipi.go.id/index.php/reinwardtia/article/view/402)
335 [journal.biologi.lipi.go.id/index.php/reinwardtia/article/view/402](https://e-journal.biologi.lipi.go.id/index.php/reinwardtia/article/view/402) (Accessed November 22, 2021)
336
- 337 O'Byrne, P. (2017). A taxonomic revision of *Dipodium* section *Leopardanthus*. *Malesian Orchid*
338 *Journal* 19, 5–142.
339
- 340 Peltier, G., Aro, E-M., Shikanai, T. (2016). NDH-1 and NDH-2 plastoquinone reductases in oxygenic
341 photosynthesis. *Ann. Rev. Plant Biology* 67, 55–80. doi.org/10.1146/annurev-arplant-043014-114752
342
- 343 Peng, H.-W., Lian, L. Zhang, J., Erst A.S., Wang, W. (2022). Phylogenomics, plastome degradation
344 and mycoheterotrophy evolution of Neottieae (Orchidaceae), with emphasis on the systematic position
345 and Loess Plateau-Changbai Mountains disjunction of *Diplandrorchis*. *BMC Plant Biol.* 22, 5077.
346 doi.org/10.1186/s12870-022-03906-0
347
- 348 Pérez-Escobar, O. A, Bogarín, D., Przelomska, N.A.S., Ackerman, J.D., Balbuena, J.A., Bellot, S.
349 Bühlmann, R. P., Cabrera, B., Aguilar Cano, J. , Charitonidou, M., Chomicki, G., Clements, M.A.,
350 Cribb, P., Fernández, M., Flanagan, N.S., Gravendeel, B., Hágsater, E., Halley, J.M., Hu, A.-Q.,
351 Jaramillo, C., Mauad, A.V., Maurin, O., Müntz, R., Leitch, I.J., Li, L., Negrao, R., Osés, L., Phillips,
352 C., Rincon, M. Salazar-Chavez, G., Simpson, L., Smidt, E., Solano-Gomez, R., Parra-Sánchez, E.,
353 Tremblay, R.L., van den Berg, C., Villanueva, B.S., Zuluaga, A., Chase, M.W., Fay, M.F., Condamine,
354 M.F., Forest, F. Nargar, N., Renner, S. S., Baker, W.J., Antonelli, A. (2023). The origin and speciation
355 of orchids [Preprint]. Available at <https://www.biorxiv.org/content/10.1101/2023.09.10.556973v3.full>,
356 (Accessed January 3, 2024). doi.org/10.1101/2023.09.10.556973
357
- 358 POWO (2023). Plants of the World Online. Facilitated by the Royal Botanic Gardens, Kew. Published
359 on the Internet; <http://www.plantsoftheworldonline.org/> (Accessed September 8, 2023).
360
- 361 Pridgeon, A.M., Cribb, P.J., Chase, M.W., Rasmussen, F.N. et al. (2009). Genera Orchidacearum,
362 Volume 5, Epidendroideae (Part 2). Oxford University, Oxford (New York), 585.
363
- 364 Qu, X.J., Fan, S.J., Wicke, S., Yi, T.S. (2019). Plastome reduction in the only parasitic gymnosperm
365 *Parasitaxus* is due to losses of photosynthesis but not housekeeping genes and apparently involves the
366 secondary gain of a Large Inverted Repeat. *Genome Biol. Evol.* 11(10). 2789–2796.
367 doi.org/10.1093/gbe/evz187
368
- 369 Quilty, P.G. (1994). The background: 144 million years of Australian paleoclimate and
370 palaeogeography. In 'History of the Australian vegetation: Cretaceous to recent'. 14–39. 2017 Edition.
371 (Cambridge University Press: Cambridge, UK). doi.org/10.20851/australian-vegetation
372

- 373 Rambaut, A., Drummond, A.J., Xie, D., Baele, G., Suchard, M.A. (2018). Posterior summarization in
374 Bayesian phylogenetics using Tracer 1.7. *Syst. Biol.* 67, 901–904. doi.org/10.1093/sysbio/syy032
375
- 376 Rolland, N., Dorne, A.J., Amoroso, G., Sültemeyer, D.F., Joyard, J., Rochaix, J.D. (1997). Disruption
377 of the plastid *ycf10* open reading frame affects uptake of inorganic carbon in the chloroplast of
378 *Chlamydomonas*. *EMBO J.* 16, 6713–6726. doi.org/10.1093/emboj/16.22.6713
379
- 380 Roma, L., Cozzolino, S., Schlüter, P.M., Scopece, G., Cafasso, D. (2018). The complete plastid
381 genomes of *Ophrys iricolor* and *O. sphegodes* (Orchidaceae) and comparative analyses with other
382 orchids. *PLOS ONE* 13, e0204174. doi.org/10.1371/journal.pone.0204174
383
- 384 Ruhlman, T.A., Jansen, R.K. (2014). The plastid genomes of flowering plants. ‘Chloroplast
385 Biotechnology’. *Methods Mol. Biol.* 3–38. doi.org/10.1007/978-1-62703-995-6_1
386
- 387 Sabater, B. (2021). On the edge of dispensability, the chloroplast *ndh* genes. *Int. J. Mol. Sci.* 22, 12505.
388 doi.org/10.3390/ijms222212505
389
- 390 Schelkunov, M.I., Shtratnikova, V.Y., Nuraliev, M.S., Selosse, M.A., Penin, A.A., Logacheva, M.D.
391 (2015). Exploring the limits for reduction of plastid genomes: A case study of the mycoheterotrophic
392 orchids *Epipogium aphyllum* and *Epipogium roseum*. *Genome Biol. Evol.* 7, 1179–1191.
393 doi.org/10.1093/gbe/evv019
394
- 395 Schlechter (1911). LII. *D. gracile* Schltr. nov. spec. in *Repertorium Specierum Novarum Regni*
396 *Vegetabilis* 10: 191. Berlin, Selbstverlag des Herausgebers 1912[1911].
397
- 398 Serna-Sánchez, M.A., Pérez-Escobar, O.A., Bogarín, D., Torres-Jimenez, M.F., Alvarez-Yela, A.C.,
399 Arcila-Galvis, J.E., Hall, C.F., De Barros, F., Pinheiro, F., Dodsworth, S., Chase, M.W., Antonelli, A.,
400 Arias, T. (2021). Plastid phylogenomics resolves ambiguous relationships within the orchid family and
401 provides a solid timeframe for biogeography and macroevolution. *Sci. Rep.* 11, 6858.
402 doi.org/10.1038/s41598-021-83664-5
403
- 404 Suetsugu, K., Ohta, T., Tayasu, I. (2018). Partial mycoheterotrophy in the leafless orchid *Cymbidium*
405 *macrorhizon*. *Am. J. Bot.* 105(9): 1595–1600. doi.org/10.1002/ajb2.1142
406
- 407 Sun, Y., Moore, M.J., Lin, N., Adelalu, K.F., Meng, A., Jian, S., Yang, L., Li, J., Wang, H. (2017).
408 Complete plastome sequencing of both living species of Circaeasteraceae (Ranunculales) reveals
409 unusual rearrangements and the loss of the *ndh* gene family. *BMC Genom.* 9;18(1):592.
410 doi.org/10.1186/s12864-017-3956-3
411
- 412 Tamura, K., Stecher, G., Kumar, S. (2021). MEGA11: Molecular evolutionary Genetics Analysis
413 Version 11 (FU Battistuzzi, Ed.). *Mol. Biol. Evol.* 38, 3022–3027. doi.org/10.1093/molbev/msab120
414
- 415 Thode, V.A., Lohmann, L.G. (2019). Comparative chloroplast genomics at low taxonomic levels: A
416 case study using *Amphilophium* (Bignoniaceae, Bignoniaceae). *Front. Plant Sci.* 10, 796.
417 doi.org/10.3389/fpls.2019.00796
418
- 419 Tu, X.D., Liu, D.K., Xu, S.W., Zhou, C.Y., Gao, X.Y., Zeng, M.Y., Zhang, S., Chen, J.L., Ma, L., Zhou,
420 Z., Huang, M.Z., Chen, S.P., Liu, Z.J., Lan, S.R., Li, M.H. (2021). Plastid phylogenomics improves
421 resolution of phylogenetic relationship in the *Cheirostylis* and *Goodyera* clades of Goodyerinae
422 (Orchidoideae, Orchidaceae). *Mol. Phyl. Evol.* 164, 107269. doi.org/10.1016/j.ympev.2021.107269
423
- 424 Wen, Y., Qin, Y., Shao, B., Li, J., Ma, C., Liu, Y., Yang, B., Jin, X. (2022). The extremely reduced,
425 diverged and reconfigured plastomes of the largest mycoheterotrophic orchid lineage. *BMC Plant Biol.*
426 22, 448 (2022). doi.org/10.1186/s12870-022-03836-x
427

- 428 WFO (2023). World Flora Online. Available at: <http://www.worldfloraonline.org> (Accessed in
429 September 2023)
430
- 431 Wicke, S., Müller, K., De Pamphilis, C., Quandt, D., Bellot, S., Schneeweiss G (2016). Mechanistic
432 model of evolutionary rate variation en route to a nonphotosynthetic lifestyle in plants. *Proc. Nat. Acad.*
433 *Sci.* 113 (32), 9045–9050. doi.org/10.1073/pnas.1607576113
434
- 435 Wicke, S., Naumann, J. (2018). Molecular evolution of plastid genomes in parasitic flowering plants.
436 *Adv. Bot. Res.* 85, 315–347. doi.org/10.1016/bs.abr.2017.11.014
437
- 438 Wu, S., Chen, J., Li, Y., Liu, A., Li, A., Yin, M., Shrestha, N., Liu, J., Ren, G. (2021). Extensive
439 genomic rearrangements mediated by repetitive sequences in plastomes of *Medicago* and its relatives.
440 *BMC Plant Biol.* 21, 421. doi.org/10.1186/s12870-021-03202-3
441
- 442 Yamori, W., Shikanai, T., Makino, A. (2015). Photosystem I cyclic electron flow via chloroplast NADH
443 dehydrogenase-like complex performs a physiological role for photosynthesis at low light. *Sci. Rep.* 5,
444 13908. doi.org/10.1038/srep13908
445
- 446 Yang, J.B., Tang, M., Li, H.T., Zhang, Z.R., Li, D.Z. (2013). Complete chloroplast genome of the genus
447 *Cymbidium*: lights into the species identification, phylogenetic implications and population genetic
448 analyses. *BMC Evol. Biol.* 13, 84. doi.org/10.1186/1471-2148-13-84
449
- 450 Yule, G.U. (1925). A mathematical theory of evolution, based on the conclusions of Dr. J. C. Willis,
451 F.R.S. *Philos. Trans. R. Soc. B Biol. Sci.* 213, 21–87. doi:10.1098/rstb.1925.0002
452
- 453 Zhang, G., Hu, Y., Huang, M.Z., Huang, W.C., Liu, D.K., Zhang, D., Hu, H., Downing, J.L., Liu, Z.J.,
454 Ma, H. (2023). Comprehensive phylogenetic analyses of Orchidaceae using nuclear genes and
455 evolutionary insights into epiphytism. *J. Integr. Plant Biol.* 65(5), 1204–1225.
456 doi.org/10.1111/jipb.13462
457
- 458 Zuckerkandl, E., Pauling, L. (1965). Molecules as documents of evolutionary history. *J. Theor. Biol.* 8,
459 357–366.